Energy Technology
Generation, Conversion, Storage, Distribution
www.entechnol.de

Different Dimensional Nanostructured Silicon Materials: From Synthesis Methodology to Application in High-Energy Lithium-Ion Batteries

Lin Sun, Jie Xie, and Zhong Jin**

Nanostructured silicon is regarded as one of the most promising next-generation anode materials for lithium-ion batteries (LIBs) due to its high capacity and proper working voltage. However, the complexity in preparing nanostructured silicon and the large volume change in silicon during lithiation and delithiation impedes its commercial application. Herein, the recent progresses relating to nanostructured Si-based anode materials are reviewed. The preparation of nanostructured silicon from dimensionality and methodology is mainly focused on, and the impactful works on silicon-based anodes, as well as the recent research directions in this field, are outlined. Finally, key lessons from the successes so far are reviewed, and further perspectives to enable the application of silicon-based anodes in practical LIBs are offered.

1. Introduction

As one of the semiconducting materials with outstanding properties, silicon (Si) has been widely used in a variety of applications in semiconductor technology development. Especially in the photovoltaic industry, more than 90% of photovoltaic cells are exploited based on Si building blocks.[1] In addition, Si is the second-most abundant element of the Earth's crust and is considered to be limitless in supply, which will significantly lower the potential cost. In recent years, porous materials have been in the spotlight of research areas, ranging from adsorption, separation, to catalysis due to their huge specific surface area and ordered micro-, meso-, and macropores. Thus, the preparation and application of porous silicon (pSi) have also attracted researchers' interests.[2] However, up to now, there have been few reports related to the effective and facile preparation of pSi, which is attributed to the high activity of pSi with a high surface area, as well as the limited preparation approaches. Alternatively, people turned to focus on the synthesis of Si nanoparticles (Si NPs). (In many situations, Si NPs exhibit comparable performances when compared with pSi; also, in contrast to the preparation of pSi, it is relatively toilless to obtain Si NPs.)

It is well known that Si-based anodic lithium-ion batteries (LIBs) represent a kind of energy storage device with ultrahigh lithium storage capacity when compared with traditional graphite ones. However, Si suffers from huge volume changes during lithiation and delithiation, thus easily resulting in the pulverization of the electrode and unstability of the formed solid electrolyte interphase (SEI) film. Common approaches to dealing with the problem include the nanomerization of bulk Si materials as well as the rational design of some unique Si structures to confront with the aforementioned issues. Certainly, controllable design and preparation of nanomaterials with low cost and in facile conditions are always the key and fundamental issues needed to be addressed in the process of commercialization. Moreover, there are many curious phenomena within nanomaterials, such as size and quantum confinement effects, which can significantly change their physical and chemical properties, thus making such materials have huge potential applications in the fields of optoelectronics, sensors, biology, etc.[3] In the past few years, many highlighted works have been conducted to prepare multifunctional Si for LIB applications, so it is necessary and important to summarize these works. This review will illustrate a brief scope in recent years, covering the various preparation methods of Si nanomaterials in different dimensions and their applications as anodes in LIBs.

2. Current Development Trends of Si Nanomaterials

Theoretically, Si should be featured with low cost because of its abundance. However, the current market price of Si nanomaterials

Dr. L. Sun, J. Xie
School of Chemistry and Chemical Engineering
Jiangsu Collaborative Innovation Center for Ecological Building Materials and Environmental Protection Equipments
Yancheng Institute of Technology
Yancheng 224051, P. R. China
E-mail: chem_sun@ycit.edu.cn

J. Xie
School of Petrochemical Engineering
Changzhou University
Changzhou 213164, P. R. China

Dr. L. Sun, Prof. Z. Jin
Key Laboratory of Mesoscopic Chemistry of MOE
School of Chemistry and Chemical Engineering
Nanjing University
Nanjing 210023, P. R. China
E-mail: zhongjin@nju.edu.cn

The ORCID identification number(s) for the author(s) of this article can be found under https://doi.org/10.1002/ente.201900962.

DOI: 10.1002/ente.201900962

is very expensive, which is mainly attributed to the extremely rare form of Si, in the form of elementary substance. Alternatively, the forms of existence of Si in nature are usually oxides and complex silicates. As we know, it is very difficult to obtain elementary Si from these oxides and complex silicates because of the huge energy needed when breaking the chemical bonds such as Si—O and Si—Cl. Moreover, it should be indicated that the soluble and effective precursors that can be used to prepare Si are very limited. From views of applications, as one of the most important electrical materials in industry, Si is an indirect band-gap semiconductor with outstanding properties and has been widely used in logical switches, sensors, solar cells, etc.[4] Nonetheless, the photon adsorption and emission processes of Si are usually related to phonons. Therefore, Si will transform the adsorbed photo-energy into lattice vibrational heat energy, which will further lead to low luminous efficiency. Thus, Si is usually not regarded as the ideal building block for fabricating photoelectric devices.

Monocrystalline Si has already proved its values in the field of photovoltaics. Although bulk Si is not suitable for fabricating luminescent devices, in the past few years, researchers found that Si NPs (or Si quantum dots [Si QDs]) are effective fluorescent materials. For example, as shown in **Figure 1**a–c, He and coworkers modified carbazole molecules on the surface of Si QDs, elevating the fluorescence quantum yield of Si QDs up to 75%.[5] More recently, this record was refreshed once again. As shown in Figure 1d–g, Li et al. used sodium naphthalene to reduce $SiBr_4$ in glycol dimethyl ether solvent, after modifying with tetrahydrocarbazone on the obtained Si NPs (particle size is ≈5.2 nm), and the fluorescence quantum yield of Si NPs reached as high as 90%, which is comparable with commercial dyes and some classical fluorescent QDs.[6]

Moreover, it should be pointed out that fluorescent Si NPs are preferred by researchers in life sciences because of the biodegradability and nontoxicity of Si. Specifically, Si NPs with luminous efficiency in red or near-infrared regions are very appropriate for diagnosing and detecting diseases.[7]

In the past decade, Si-based nanomaterials have received a lot of attention in energy areas, especially as anodes in rechargeable LIBs. Si anodic LIBs deliver a theoretical capacity of ≈4200 mA h g^{-1}, which is ≈11 times than that of commercial graphite ones.[8] However, the cyclic performance of Si anodes is usually not satisfied because Si exhibits volume changes of ≈300% upon lithium alloying and dealloying, which will result in fracture and loss of the electrical contact and growth of an unstable SEI on the Si surface. To tackle the issue, Si NPs have been used as anode materials for LIBs because nanoscaled structures with large surface areas and abundant interspaces between particles not only effectively address the pulverization problem of the Si anodes, but also allow high operation rates.

3. Classifications of Nano-Si Materials

Nanomaterials are typically classified into 0D NPs (including QDs), 1D nanowires (NWs) or nanotubes, 2D nanosheets, and 3D porous materials from a size perspective. Similarly, Si nanomaterials can also be classified from a dimensional perspective.

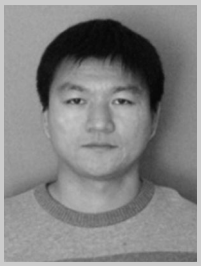

Lin Sun received his B.S. degree in chemical engineering in 2010 from the Department of Chemistry and Chemical Engineering, Yancheng Institute of Technology, and his M.Sc. degree in chemical engineering from the School of Petrochemical Engineering, Changzhou University. He obtained his Ph.D. degree in chemistry from Nanjing University. His research interests are focused on preparing organic/inorganic porous materials of importance in adsorption, separation, catalysis, optoelectronics, and energy science using new synthetic methods and strategies under the guidance of modern computational chemistry.

Jie Xie received his B.S. degree from the School of Chemistry and Chemical Engineering at Yancheng Institute of Technology in 2018. He is currently a master's candidate under the supervision of Dr. Lin Sun in the School of Petrochemical Engineering at Changzhou University. His research is mainly focused on the synthesis of energy storage and conversion functional materials.

Zhong Jin received his B.S. (2003) and Ph.D. (2008) degrees in chemistry from Peking University. He worked as a postdoctoral scholar at Rice University and Massachusetts Institute of Technology. He is now a professor in the School of Chemistry and Chemical Engineering at Nanjing University. He leads a research group on functional nanomaterials and devices for energy conversion and storage.

3.1. 0D Silicon Particles

The size of 0D Si NPs is less than 100 nm, because the 0D material has a particularly obvious quantum confinement effect, especially the Si QDs, and their sizes are only a few nanometers. Moreover, the photoelectrical property of Si is greatly changed when its size is close to the Bohr radius (about 4 nm) because of its indirect band-gap feature. More importantly, Si is a biocompatible substance; therefore, the merits of Si QDs have attracted much attention in life science such as cell imaging, biological probe, and drug transportation. In recent years, a series of methods for synthesizing Si QDs have been developed, among which the most common and relatively popular ones are solution-based syntheses such as chemical reduction[9] and microwave synthesis.[10] The chemical reduction method is a direct reduction of surface-exposed or protected Si QDs by a strong reducing agent in the presence of an organosilane in a certain organic solvent. As early as 1992, Heath first used this method to obtain

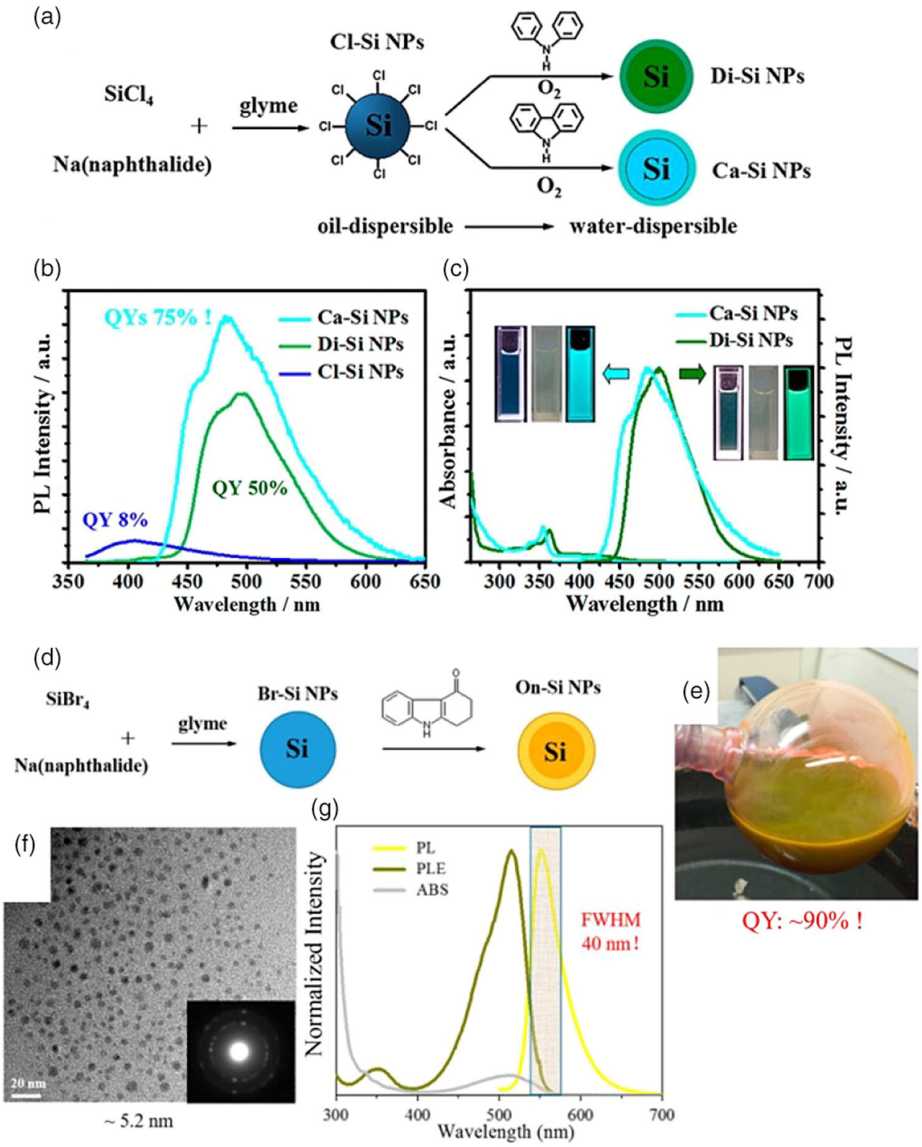

Figure 1. a) Scheme of solution reduction syntheses and surface modification to prepare highly luminescent water-dispersible SiNPs. b) PL spectra of SiNPs before and after surface modification. c) Normalized PL and UV–Visible absorption spectra of the two surface-modified SiNPs. d) Scheme of modified Si QDs with ultrahigh fluorescence quantum yield via solution reduction method. e) Optical photo of On–Si dispersing in glycol dimethyl ether. f) TEM image of On–Si. g) Photoluminescence (PL), photoluminescence excitation (PLE) and absorption spectra (ABS) of On–Si. (a–c) Reproduced with permission.[5] Copyright 2013, American Chemical Society. (d–g) Reproduced with permission.[6] Copyright 2016, American Chemical Society.

crystal silicon via reducing $SiCl_4$ or $RSiCl_3$ by metal sodium in a nonpolar organic solvent under high temperature and high pressure (385 °C more than 100 atmospheres).[11] A series of preparation methods based on simple chemical reduction have been developed. As shown in **Figure 2**,[12] $SiCl_4$ is usually used as a Si source in an ether solvent, and $LiAlH_4$ and $NaC_{10}H_8$ are generally used as reducing agents. At the same time, the prepared Si QDs can also be protected by surface passivation by adding some protective groups. In addition, a modified chemical substitution method is also a relatively common strategy for preparing Si QDs. Zintl compounds such as KSi, NaSi, or Mg_2Si are used as Si sources, and Si QDs are obtained by reacting a corresponding Si halide or Br_2, NH_4Br, as well as the like as an oxidizing agent at room temperature or under heating for a sufficient period of time.[13]

Microwave-assisted synthesis is a popular method for synthesizing functional QDs.[14] At the same time, the synthesis of Si QDs by the microwave method has also been widely used. One of the biggest advantages of microwave-assisted methods is that it can greatly shorten the reaction time under the microwave condition, and a large amount of functional nanomaterials can be obtained in a short time. Although the mechanism of microwave-assisted synthesis of nanomaterials is still not very clear at present, this method can indeed provide a shortcut for the synthesis of functional nanomaterials. For example, as shown in **Figure 3**, Ye et al. obtained Si QDs with the maximum emission

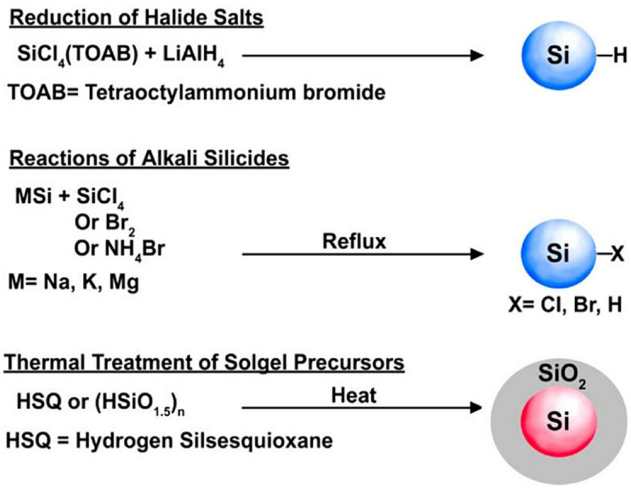

Figure 2. Preparation of surface-functionalized Si QDs based on chemical reduction method. Reproduced with permission.[12] Copyright 2014, American Chemical Society.

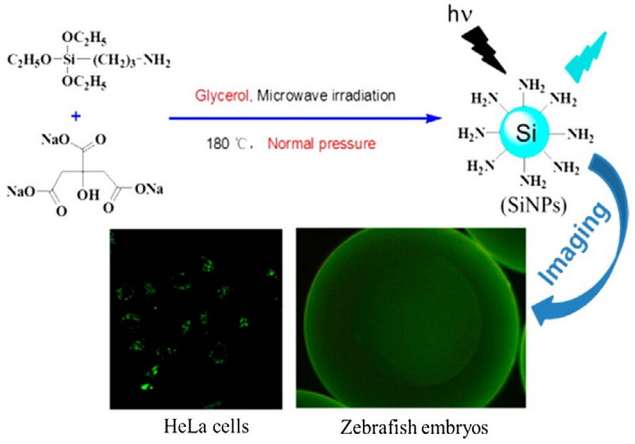

Figure 3. Schematic illustration of Si NP synthesis. Reproduced with permission.[15] Copyright 2016, American Chemical Society.

wavelength of ≈660 nm by adding glutaric acid under a microwave-assisted reaction at 185 °C for 10 min.[15] The obtained Si QDs have a very narrow size distribution of about 4.5 nm. In addition, Si QDs can also be synthesized by other less common methods, such as the hydrothermal method,[16] self-assembly,[17] the cosputtering method,[18] supercritical fluid preparation,[19] and high-temperature laser synthesis.[20]

3.2. 1D Silicon Nanowires

1D Si NWs have received wide attention in both physical and chemical fields due to their unique structures. The reason why people are interested in Si NWs is mainly because they have many novel unique properties such as optoelectronics, magnetism, and mechanics, which are significantly different from other low-dimensional semiconductor materials, which make them possess huge potential applications in field-effect devices, single-electron memory devices, photodetector devices, sensors, and luminescent materials.[21] As early as 1964, Wagner et al. first synthesized Si NWs by the vapor–liquid–solid (VLS) method.[22] It is considered that the synthesis of Si NWs by VLS method is one of the most earliest and mature synthesis strategies, and a large series of relevant methods have been developed so far, such as the chemical vapor deposition (CVD) method, physical evaporation method, and other similar ones. The mechanism of the VLS method can be explained by the following Si–Au binary phase diagram (**Figure 4**).[23] First, the Si is formed by the cleavage of the Si—Si bonds in precursors to form a eutectic droplet above the eutectic point of ≈363 °C on the Au particles growing on the substrate. When Si atoms that continue to be cleaved fall onto this droplet, the Si atoms therein will reach saturation. The Si NWs are formed by gradually growing in one direction according to the principle of lowest energy. In this mechanism, metals play very important roles in nucleation, so people can prepare Si NWs with different diameters by regulating metal species and temperature.

Based on the VLS reaction mechanism, various Si nanotubes and NWs have been synthesized so far. The synthesis methods are also diverse, such as CVD,[24] in which VLS-based metal-catalyzed CVD is more common, and metal-assisted solution etching.[25] These two methods were regarded as the typical "bottom-up" and "top-down" strategies for the preparation of Si NWs. In CVD methods, silane and silicon halide are generally used as precursors to prepare Si NWs by thermal decomposition at a high temperature. All key indicators of NWs such as chemical composition, diameter, length, and doping can be precisely controlled by regulating the crystal growth environment. For example, the thinnest NWs are currently known to be only a few nanometers,[26] and the longest NWs can reach a few millimeters.[27]

At present, the mainstream process for preparing Si NWs should be metal-catalyzed VLS growth. In the implementation of this process, one of the active metals (such as Au, Fe, Ni or Al, etc.) is first deposited on the Si substrate by sputtering or evaporation and then heated, using the eutectic action of the metal and Si substrate to form alloy droplets.[28] Thereafter, by the vapor phase transport of the source gas containing Si or the thermal evaporation of the solid target, atoms participating in the formation of the Si NWs are agglomerated

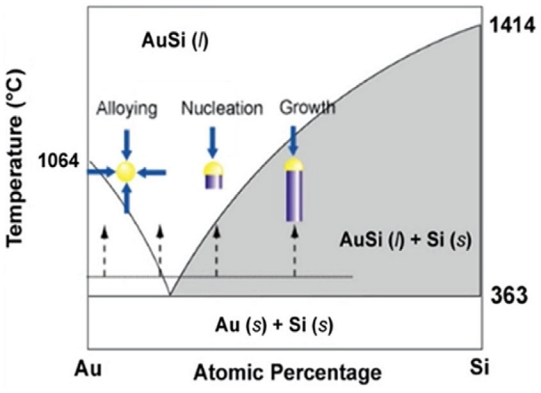

Figure 4. Binary phase diagram of Si–Au. Reproduced with permission.[23] Copyright 2008, American Chemical Society.

into nuclei at the droplets, thereby forming Si NWs with a certain shape, diameter, and length in a certain direction. Compared with gas phase synthesis, solution synthesis can effectively regulate the structural properties and preparation conditions of nanomaterials. Therefore, based on the classical VLS growth theory, a method for preparing Si NWs based on solid–liquid–solid (SLS) and supercritical fluid–liquid–solid (SFLS) has also been developed in the past two decades. As early as 2000, Si NWs with a length-to-diameter ratio of 1000 were prepared by Korgel's group at 500 °C and 200 to 270 bar using Au nanocrystals with a size of about 2.5 nm as seeds and diphenylsilane as the Si source.[29] At the same time, the crystal orientation of the obtained Si NWs can be controlled by regulating the pressure. Clearly, the synthesis conditions at 500 °C and 270 bar pressure are still too harsh. In 2008, based on the SLS growth mechanism, Si_3H_8 was used as the Si source, and nano-Au or Bi was used as the seed. Si NWs were grown under normal pressure conditions in a solution of octadecane or pin squalane.[30]

Metal-assisted solution etching is a typical synthesis method using the "top-down" strategy. A common and low-cost method is utilized to deposit a layer of nanoprecious metal such as Ag on the surface of a single-crystal Si substrate. This layer of precious metal can greatly accelerate the redox reaction rate of the inner Si that is in contact with it. As the reaction progresses, the bulk Si is etched to form a NW array. The etching solution usually involves HF and H_2O_2, and as this method is simple in operation, it is widely used for large-scale production of Si NWs.[31]

Recently, Rey et al. integrated the "bottom-up" and "top-down" synthesis strategies and invented a "soft NP template" technique to synthesize Si NW arrays with controllable length, site, and spacing.[32] As shown in **Figure 5**, monodispersed microgel particles are grown at the water–n-hexane interface, the microgel particles being compressible (because of the coated cross-linked and water-soluble polymers). Figure 5a,b shows the states of the surface microgel particles at the water and water–oil interface, respectively, and c and d shows the alignment of the microgel particles from top down. By inserting the Si substrate into the water–oil solution containing the microgel particles at different angles, the microgel particles at the water–oil interface are plated with the Si substrate, the arrangement pitch of the microgel particles on the Si substrate can be controlled by controlling the difference in the insertion angle (changing the surface pressure). Under photolithography, the microgel particles on the Si substrate become swollen (growth to a certain height), as shown in Figure 5e,f. Then, a 10 nm-thick layer of Au (Figure 5g) is applied to the surface. This microgel particle provides a tunable nanotemplate for growing Si NWs and grows regular NW arrays (Figure 5h). The main advantage of this method is that it can precisely regulate the growth site of the NW array and the distance between the lines and the line.

3.3. 2D Si Nanosheets

Due to the ultrathin structure and unique optoelectronic properties, 2D materials such as graphene and MoS_2 have attracted much attention.[33] Compared with graphene, the synthesis of 2D Si nanosheets is restricted mainly due to the limitations of Si sources and preparation methods. It should be realized that synthesizing Si sheets with single atomic layer thickness is very difficult. The current reported strategies for obtaining Si nanosheets are generally based on CVD methods. For example, Kim et al.[34] used H_2 as a carrier gas and introduced $SiCl_4$ into a CVD furnace at 1000 °C to prepare Si nanosheets with a thickness of ≈2 nm without any catalysts, and meanwhile the luminescence properties were investigated; the results are shown in **Figure 6**. However, in general, 2D Si prepared by this method is complex, and the thickness cannot be precisely controlled, and it is difficult to exert the optimal performance of the 2D material.

It is pointed out that the solution method has always been on the spotlight for preparing nanomaterials because of the feasibility in operation, the mild and uniform reaction condition, and being relatively easy for large-scale production. Considering that $CaSi_2$ is a layered Zintl compound, if the Si layer and the Ca layer can be separated by a certain methodology, it is nonetheless a good way for preparing 2D Si nanostructures. Yamanaka et al.[35] developed a method for stripping $CaSi_2$ in a strong acid (concentrated hydrochloric acid) system as early as 1996 and studied the effects of reaction temperature, acid concentration, and reaction time on the product in detail. The results show that no obvious oxygen can be detected on the surface of the Si sheets obtained by the reaction at −30 °C for about 1 week. Instead, the surface H-passivated Si_6H_6 nanosheet is obtained. However, due to the instability of the Si—H bond, further surface modification should be conducted on the basis of the Si_6H_6 nanosheet, and some related works have been performed.[36] Recently, our group has also developed a novel solvothermal method to prepare ultrathin SiO_x nanosheets and investigate their applications in high-energy LIBs with long lifetimes.[37]

Instead of the exfoliation of Zintl compound $CaSi_2$ to produce Si-based nanosheets, some unusual strategies can also be used. Recently, Ryu et al.[38] used natural montmorillonite as raw material to synthesize Si nanosheets with a thickness of 5 nm in two steps. First of all, montmorillonite and nitrate are ground and heat treated at 250–320 °C (prestripping stage). Then, the obtained prestripped montmorillonite was mixed with Mg powder and NaCl, and a thin Si nanosheet was obtained by secondary peeling of NaCl and Mg thermal reaction. Similarly, as a comparison, direct reduction of montmorillonite by Mg thermal method can only obtain broken Si NPs without obtaining 2D structures. After carbon modification, the C-SiNS composite anode exhibits excellent cycling stability after cycling at different current densities; the results are shown in **Figure 7**a,b. A similar route for producing Si nanosheets can also be applied in natural vermiculite,[39] as shown in Figure 7c,d.

3.4. 3D Silicon Porous Si Materials

In addition to 0D, 1D, and 2D materials, 3D porous materials have always been the focus of researchers. For porous materials, the pores themselves are attractive enough; especially in the field of catalysis, porous materials featured with rich pore types and high specific surface areas have very large impacts on performance.[40] Among them, Si porous materials have always been the "star" substances with people's awareness of health and the importance of life sciences. The integration of nanotechnology and life sciences makes pSi a powerful tool for diagnosing

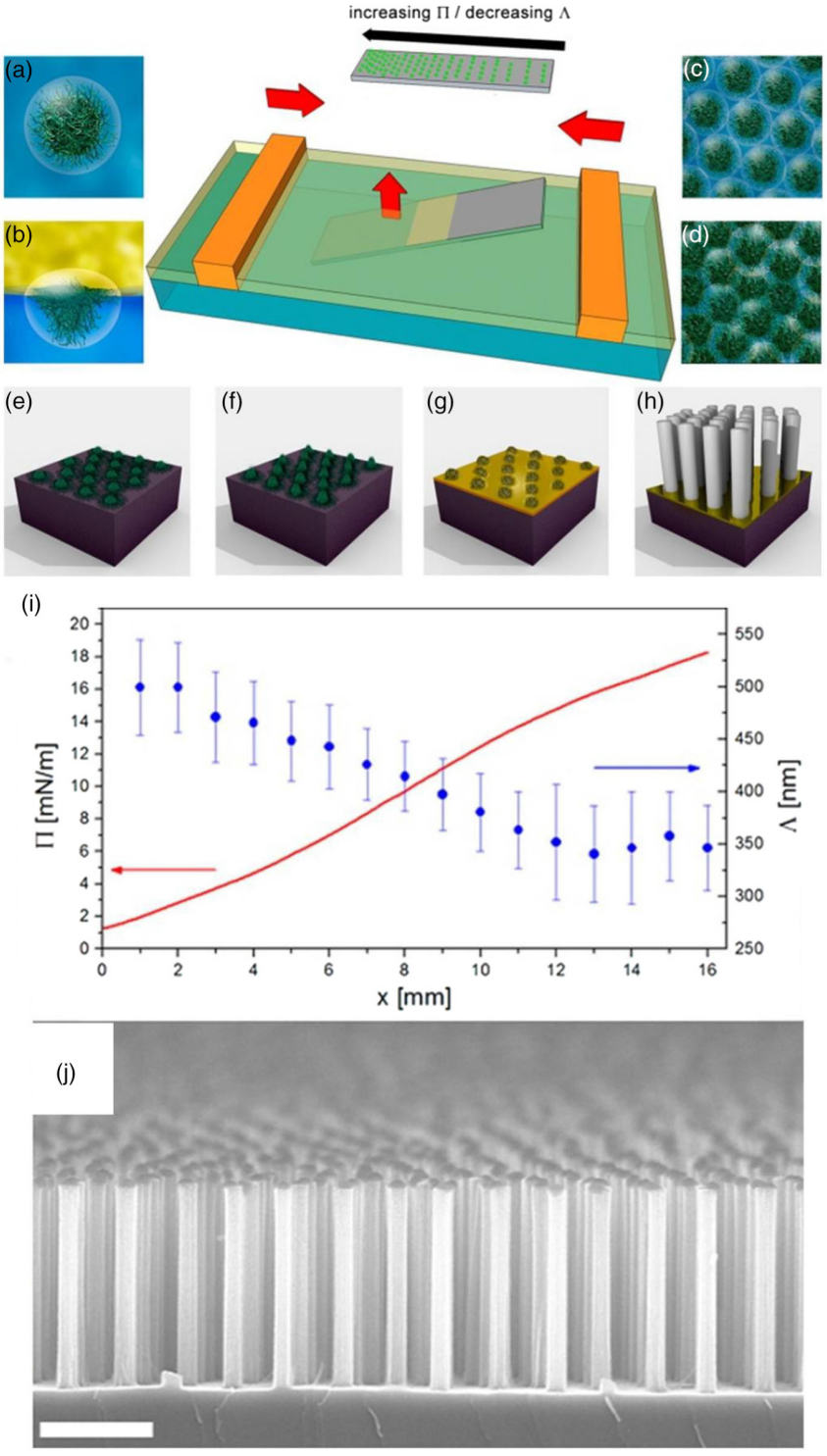

Figure 5. a,b) A schematic illustration of microgel particles in bulk water and at an oil/water (o/w) interface, respectively. c,d)Top view of the structure of the gel monolayer at different degrees of compression. The deposited microgel array e) is swollen in photoresist, leading to an increased particle height from the substrate. f) A 10 nm layer of Au is deposited and g) the microgels provide masking for the contact between the Au layer and the Si substrate. h) Upon exposure to the etching solution, the metal-assisted chemical etching (MACE) reaction proceeds around the swollen microgels, causing the formation of VA-Si NWs that replicate the lateral geometry of the customized microgel shadow mask with high fidelity. i) Center-to-center NW separation and corresponding pressure as a function of position *x* on the substrate. j) SEM cross-section of the VA-Si NW array, scale bar 1 µm. Reproduced with permission.[32] Copyright 2016, American Chemical Society.

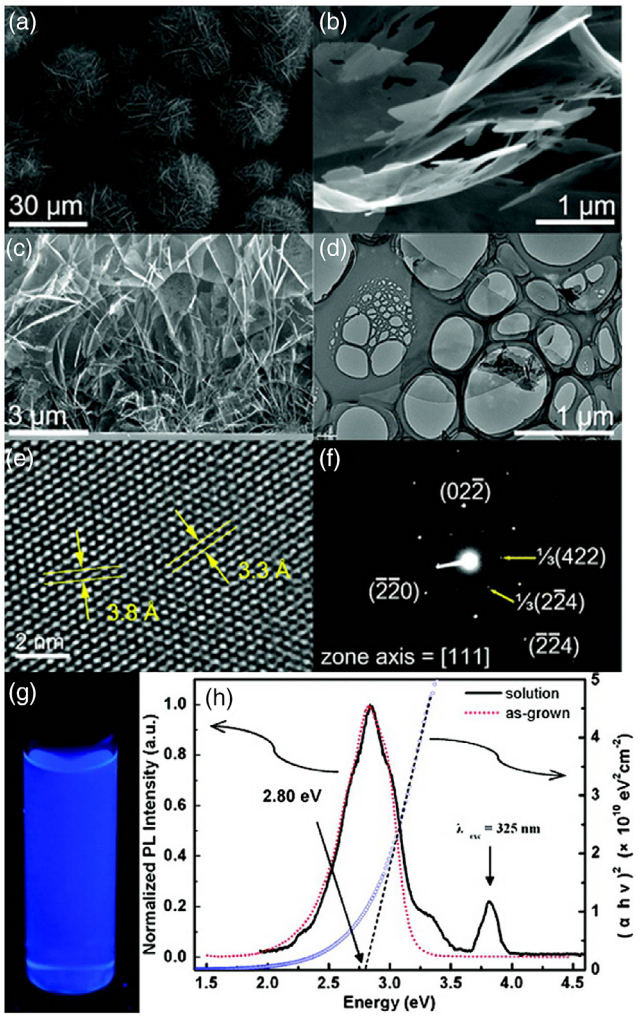

Figure 6. a,b) SEM images of Si Nanosheet (NSs) grown on a Si substrate with a growth time of 30 min. c) SEM image of cross-sectioned substrate. d) A typical low-magnitude TEM image of Si NSs. e) A high-resolution transmission electron microscopy (HRTEM) image of Si NSs, showing the single-crystalline nature of the Si NS. f) Selected area electro diffraction (SAED) pattern of Si NSs. g) The image exhibiting the luminescent emission from an ethanol solution containing Si NSs when irradiated with UV light. h) Room-temperature photoluminescence (PL) spectra of Si NSs dispersed in an ethanol solution (black, solid) and as-grown Si NSs (red, dotted) excited by a wavelength of 325 nm using a He–Cd laser. Reproduced with permission.[34] Copyright 2011, American Chemical Society.

diseases. In the field of life sciences, drug transportation is inseparable from the help of porous nanomaterials, and pSi is biocompatible, which greatly expands their application ranges.

The synthesis of pSi materials can be roughly classified into two types: "dry method" and "wet method". The so-called "dry method" is through solid phase synthesis, such as CVD, ion/plasmon etching, and hard template methods commonly used in the field of microelectronics.[41] For example, Fan et al.[42] prepared a Si/C composite via spray drying by dispersing Si NPs with particle size ranging from 80 to 160 nm in aqueous solution containing a certain amount of glucose and NaCl; as shown in **Figure 8**, Si/C materials with different carbon contents can be prepared by controlling the amount of glucose. pSi materials with different pore distributions can be obtained by controlling the amount of NaCl used.

For another example, as shown in **Figure 9**, Wang et al.[43] mixed SiO_2 and NaCl uniformly and reduced SiO_2 to elemental Si by Mg thermal reduction. The inorganic salts of NaCl and in situ-formed MgO were used as hard templates and subsequently washed away to produce disordered pSi material. The obtained compound has a high specific surface area of around 242 $m^2 g^{-1}$. The pSi material and the C nanotubes are combined to exhibit excellent electrochemical performance as a negative electrode of lithium batteries. The battery is charged and discharged at a current density of 0.5 °C for 500 cycles, the capacity degradation is less than 20%, and the reversible capacity is up to 3000 Ma h g^{-1}.

The so-called "wet method" is generally based on solution methods, using chemical or electrochemical reactions combined with hard templates. For example, Dai et al.[44] used NaK alloy to reduce $SiCl_4$ in a toluene solution, and KCl and NaCl inorganic salts were used as pore-forming agents, as shown in **Figure 10**a. The elemental Si materials with mesoporous distribution are obtained by washing the inorganic salts, and the high-temperature crystallization treatment in inert atmosphere is more favorable for the stability of the channels, and the obtained crystallized Si materials exhibit a better performance for the photolysis of water to produce hydrogen.

Although the reduction of $SiCl_4$ by NaK alloy is relatively rapid, it is not suitable for practical use due to the danger and toxicity of NaK alloy. On this basis, Lin et al.[45] recently developed a solvothermal-based Mg reduction method. That is, in the ethylene glycol dimethyl ether solution, the metal Mg powder is used to reduce $SiCl_4$ under solvothermal conditions at 100 °C, and the surface-oxidized pSi is synthesized using in situ $MgCl_2$ as a pore-forming agent material. The preparation process is shown in Figure 10b.

4. Applications of Si-Based Anodes in LIBs

4.1. Current Developments in LIBs

LIB has a high specific capacity, low self-discharge rate, no memory effect, and good cycle stability. It is currently the most promising high-efficiency secondary battery. The working mechanism of LIBs is shown in **Figure 11**a. The vigorous development in LIBs has also promoted the research of its positive and negative materials, especially the research on negative materials. As shown in Figure 11,[46] at present, research on anode materials for LIBs mainly focuses on carbon materials,[47] metal oxides such as many transition metal oxides TiO_2, CuO, NiO, Fe_3O_4, SnO_2, etc.,[48] IV main group materials (Si, Ge, Sn), etc.[49] At present, the commercial LiB anode is based on graphite. As early as the 1980s, it was found that the intercalation reaction potential of lithium metal in carbon materials is close to that of Li/Li^+. Moreover, the mechanism of carbon anodes is mainly the intercalation and deintercalation of lithium ions between the carbon layers, which will not destroy the structure of the active material, and the carbon material also has superior electrical conductivity, thus endowing it excellent cycle performance. However, the

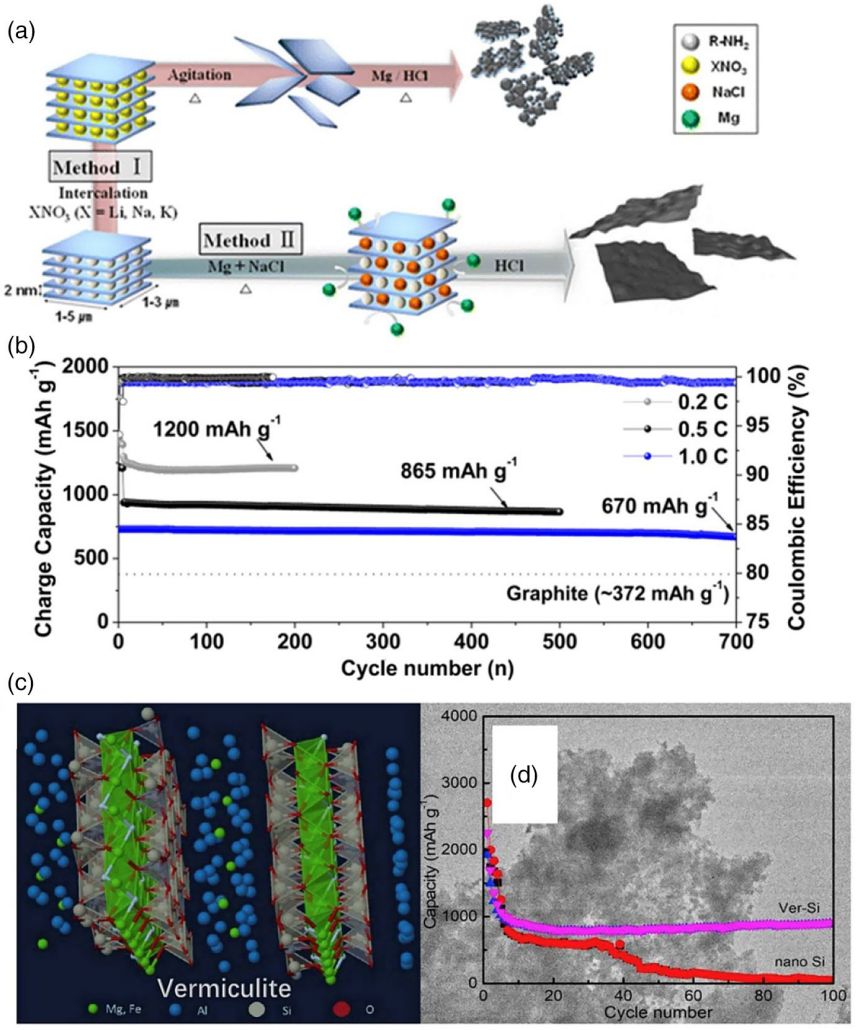

Figure 7. a) Schematic illustration shows synthetic routes for preparing Si nanosheets using two different strategies. b) Long-term cycling performance of C-SiNS electrodes at three different C rates (0.2, 0.5, and 1.0 °C). c) Scheme of the exfoliation of vermiculite. d) Cycling performance of Ver–Si and nano-Si at 0.1 A g^{-1} over 100 cycles. (a–b) Reproduced with permission.[38] Copyright 2016, American Chemical Society. (c–d) Reproduced with permission.[39] Copyright 2019, Elsevier.

drawback of carbon electrodes is that the carbon material is prone to solvent coinsertion, thereby reducing its lithium insertion performance. Moreover, the lower theoretical capacity of carbon materials (about 372 mA h g^{-1}) is gradually unable to meet the increasing demand for high energy density.

In view of this, in recent years, a series of alloy-based anodes have been developed due to their high specific capacity, such as Si, Ge, Sn, and some metal oxides as described earlier. Among them, the elemental specific capacity is up to 4200 mA h g^{-1} for elemental Si, which is 11 times than that of graphite. Moreover, the discharge potential of Si negative electrode is about 0.2 V with respect to the Li/Li^+ electrode, which is lower than that of most alloyed metal oxide anodes.[50] Regarding Si as anodes, a full battery having a high energy density can be obtained at such a low operating potential. In addition, due to the abundance of Si elements and low potential cost, among the current alloy negative electrode materials, Si has attracted the most attention.

4.2. Various Si Nanostructures as Anodes in LIBs

Nowadays, Si-based nanomaterials play very important roles in the field of energy storage and conversion. In terms of energy storage, Si as an electrode material has received extensive attention and in-depth research in the field of supercapacitors, especially in LIBs.[51] Compared with the current commercial graphite anode, Si anode is a new type of alloyed electrode material. The charge–discharge mechanism is quite different from that of graphite anode. In the process of charge and discharge, graphite anode is mainly used as a host to insert and extract Li ions between graphite layers to realize the charge and discharge process, resulting in a lower capacity (≈372 mA h g^{-1}). The alloyed negative electrode material such as Si is formed using Si and Li to form an alloy compound during charging and discharging, and one Si atom can bond more than four Li atoms, so the Si anodic lithium battery has a very high specific

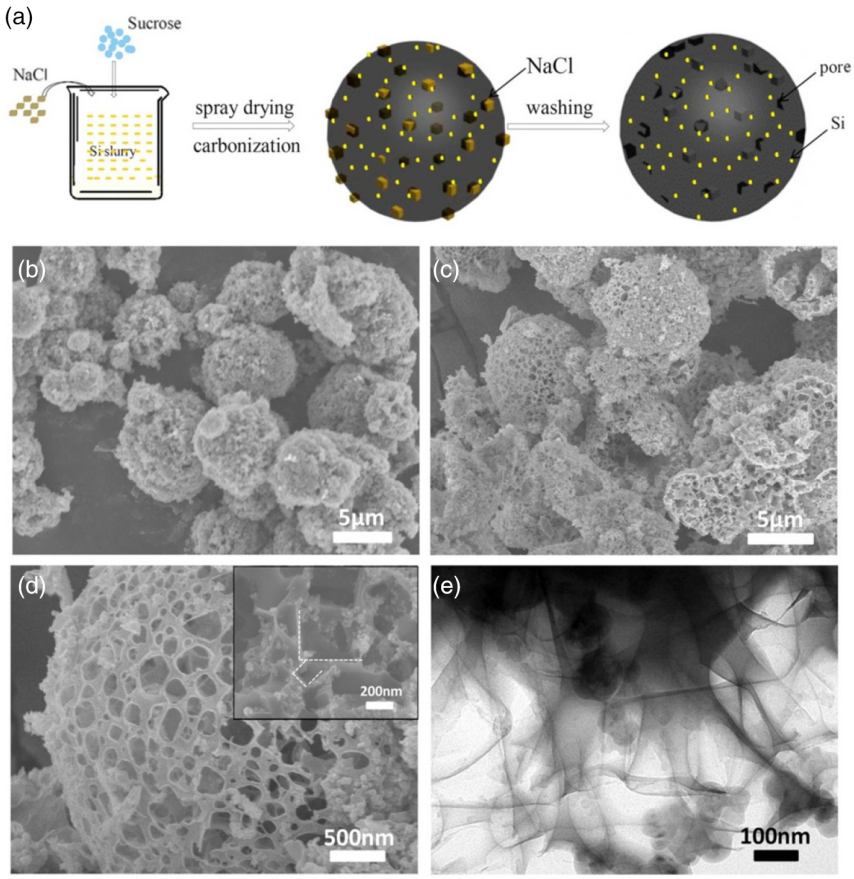

Figure 8. a) Scheme of the preparation process of pSi /C composite; b) SEM image of Si/C before washing; c,d) SEM images and e) TEM image of Si/C with different magnifications after washing; inset image in (d) presents the morphology inside Si/C. Reproduced with permission.[42] Copyright 2016, Elsevier.

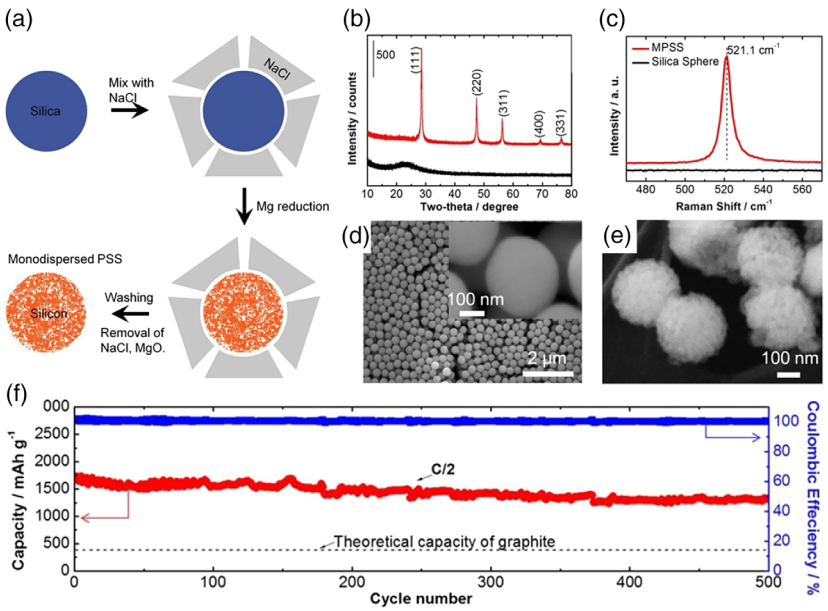

Figure 9. a) Scheme of monodisperse pSi sphere formation through surface-protected magnesiothermic reduction. b) X-ray diffraction (XRD) patterns and c) Raman spectra of solid silica spheres and monodisperse pSi. d) SEM micrographs of monodisperse solid silica spheres, inset shows the high magnification SEM micrograph of the silica sphere. e) SEM micrograph of monodisperse pSi spheres. f) Cycling performance and coulombic efficiency of monodisperse porous silicon nanospheres (MPSS) electrodes at a higher current density of C/2. Reproduced with permission.[43] Copyright 2015, Springer Nature Publishing AG.

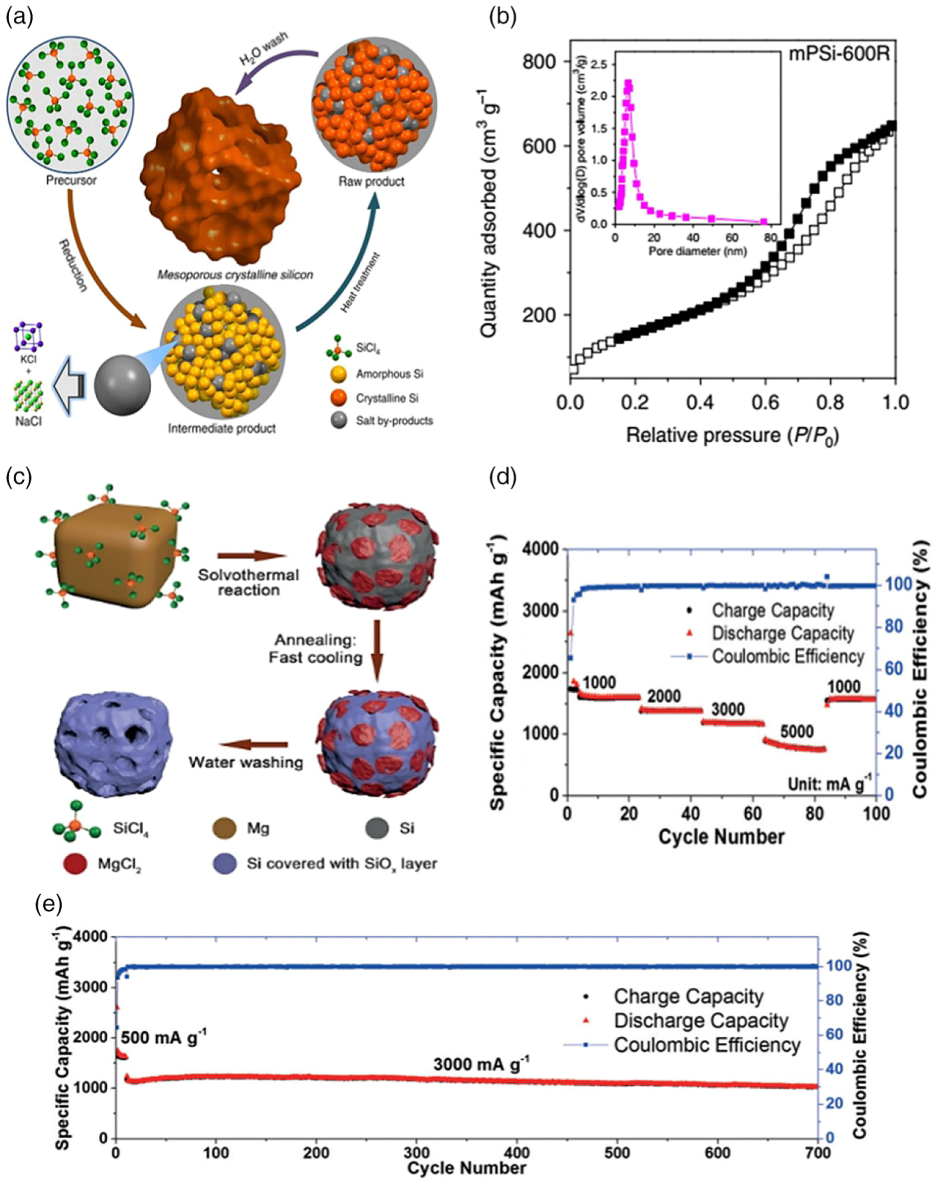

Figure 10. a) Scheme of bottom-up synthesis of mesoporous Si (mPSi). b) Nitrogen sorption isotherm and Barrett-Joyner-Halenda (BJH) pore size distribution (inset) of mPSi. c) Scheme of synthesis of porous a-Si anode. d) Rate performance and coulombic efficiency of p/a-Si at different current densities. e) Cycling performance and coulombic efficiency of p/a-Si at a current density of 3000 mA g^{-1}. (a–b) Reproduced with permission.[44] Copyright 2014, Springer Nature Publishing AG. (c–e) Reproduced with permission.[45] Copyright 2016, Wiley-VCH.

capacity. (When $Li_{4.4}Si$ is formed, the specific capacity is ≈4200 mA h g^{-1}.)[52] Such a high energy density has a very attractive application prospect; whether in aerospace, electric vehicles, or small laptops, mobile phones, etc., there is an urgent need for lithium batteries with high energy density. In addition, Si featured with a low working potential (<0.5 V), abundance in the Earth's crust, and environmental friendliness lay a solid foundation for the practical application of Si-based anode materials in the lithium battery industry.[53] However, the prospects for the application of Si-based nanomaterials in the field of lithium batteries are attractive, but there are still many practical difficulties that need to be solved (mainly in the formation of alloys, the active material itself undergoes a huge volume change, resulting in the pulverization of electrode and instability of SEI film. Meanwhile, poor conductivity and low ion and electron migration rate also result in a low rate performance). In this Review, we focus on the research progress of Si-based nanomaterials as anodes in lithium-ion secondary batteries in recent years, including the application of Si nanomaterials with different structures and the postprocessing of Si nanomaterials to solve the problems encountered in the process of charge and discharge.

Reducing or eliminating the adverse effects caused by the large volume change in the Si-based negative electrode material during charge and discharge can be realized by reducing the size

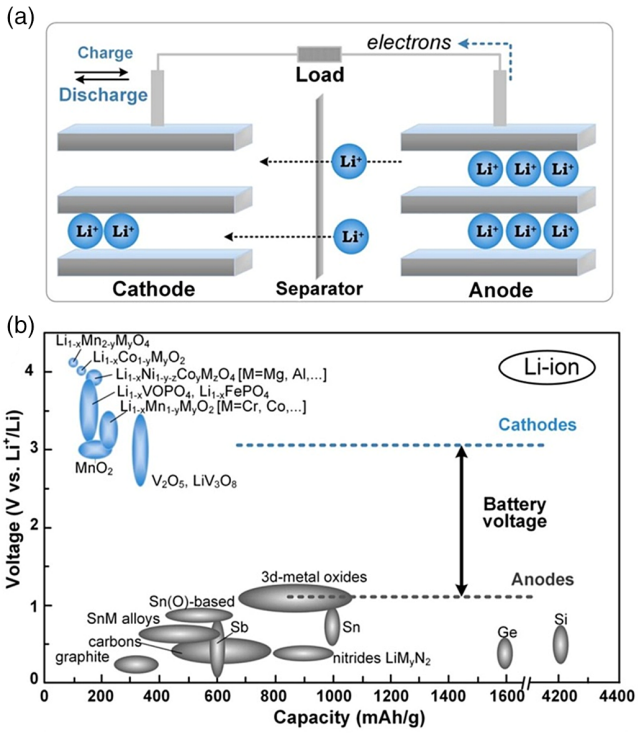

Figure 11. a) Schematic illustration of the working mechanism of LIBs. b) Classifications of positive and negative anodes in LIBs. Reproduced with permission.[46] Copyright 2014, American Chemical Society.

of bulk Si material into nanoscale. Due to the large specific surface area of the nanomaterials, the relatively large voids between the particles can form a buffer, releasing the stress caused by volume change. To this end, a series of different Si nanostructures has been synthesized to obtain electrode materials with good electrochemical properties, and the summary results are shown in **Table 1**.

4.2.1. 0D Si Nanoparticles

Si NPs are regarded as the most easily synthesized Si nanomaterials. At present, the method for industrially preparing Si NPs is generally obtained by pyrolysis of silane precursors at high temperatures via the CVD method. The obtained Si NPs have a uniform size distribution, good crystallinity, and good electrochemical performance. At present, commercial Si NPs prepared by the CVD method are generally utilized as negative electrode materials for lithium batteries. For example, Cui et al. found that the incorporation of 5 wt% polyrotaxane to conventional polyacrylic acid (PAA) binder imparts extraordinary elasticity to the polymer network originating from the ring-sliding motion of polyrotaxane. This binder combination keeps even pulverized silicon particles coalesced without disintegration, enabling stable cycle life for silicon microparticle anodes at commercial-level areal capacities,[95] as shown in **Figure 12**.

Shang et al. developed an in situ weaving strategy to apply ultrathin graphdiyne nanosheets in solving Si anodes.[96] The in situ weaving strategy greatly improves the interfacial contact among the components of the electrode. Combining with the conductivity and in-plane atomic-level cavities of graphdiyne, such a structure obtains plenty of channels for the fast migration of both electrons and ions, the scheme is shown in **Figure 13**.

As the volume of active material varies greatly during the cycle of charge and discharge of the Si negative lithium battery, the particle size of the Si NPs has a great influence on its electrochemical performance. Wang et al.[8] prepared Si QDs with a particle size of ≈3 nm and surface amination under microwave assist. The Si QDs were loaded onto the graphene sheet (GNS) surface by surface functionalization, as shown in **Figure 14**a. The obtained Si QD–GNS composite material has excellent electrochemical performance as a negative electrode of a lithium battery. The cycle stability test result of the battery is shown in Figure 14b, and at a high current density of 2 A g^{-1} and 500 cycles of charge and discharge, the Si QD–GNS negative lithium battery has almost no capacity attenuation (red line). As a comparison, the Si NPs with a particle size of ≈50 nm were directly combined with graphene, and it is shown that the capacity decays very rapidly (purple line) at a current of 2 A g^{-1}. It is shown that the size of Si particles also has a significant impact on their cycle stability. Certainly, up to now, all sorts of routes have been developed for obtaining Si or Si-based composite electrodes to enhance the electrochemical performances.[97]

4.2.2. 1D Si Nanowires

Due to the discovery and application of VLS growth mechanism, Si NWs are prone to grow on some substrates and relatively well-developed lithium battery anode material due to their good electrical conductivity.[68–71,98] As shown in **Figure 15**, as the volume change in the Si negative electrode material during the cycle charge and discharge is about four times that of itself, the Si film or the Si NPs plated on the substrate is pulverized. However, if it is a Si NW array grown on a current collector, due to the structural characteristics of the 1D material, the volume expansion coefficient in the direction perpendicular to the radial direction is small during charge and discharge, and the gap between the NWs can completely tolerate the volume change, so the Si NW can ensure the structure's stability during the electrochemical reaction. However, further studies have shown that the morphology of Si NWs during charging and discharging is not completely unaffected. Holes are formed on the surface of Si NWs after several decades of in-line lithium removal. The main reason for the formation of these pores is caused by the removal of Li from the Si–Li alloy during delithiation.[99] Cui et al.[100] found through further research that the size of these holes gradually increased with each cycle. Interestingly, they found that these holes have a "memory effect", that is, as each cycle progresses, no new holes are formed, and the shape of the original holes does not change, but the hole size gradually becomes larger. A more reasonable explanation for this is that the holes formed during the lithium intercalation process are not completely closed due to the filling of Li. Therefore, during delithiation, when the diffusion rate of Li^+ on the surface of the material is much faster than the diffusion rate of internal Li^+, the pores gradually become larger.

Table 1. Electrochemical performance of Si and their composite anodes.

2010–2019	Anode	Synthesis method	Current density [mA g^{-1}]	Discharge capacity [mA h g^{-1}]	Cycles	Capacity retention rate (%)	Ref.
Si NPs	SiQD–GNS	Solvothermal	2000	890	500	>98	[8]
	SiNP/C	Commercial	100	768	80	62.6	[54]
	SiNP/C	Commercial	1000	803	50	83	[55]
	SiNP/C	Commercial	–	626.7	10	40	[56]
	Silicon/MXene	Vacuum filtration	200	2118	100	84.7	[57]
	SiNP/Al	Al reduction	200	740	100	64.5	[58]
	SiNP/C	Mg reduction	600	954	200	74	[59]
	SiNP/G	Mg reduction	200	2050	200	51	[60]
	SiNP/C	Mg reduction	100	1250	100	90	[61]
	SiNP/C	CVD	C/2	750	100	68	[62]
	SiNP/CNT	CVD	1000	1000	100	66.7	[63]
	SiNP-C	CVD	1C	1400	100	87.5	[64]
	SiNP-C	Ball milling	1400	1508	100	70.4	[65]
	SiNP–MWCNT	Magnetron sputtering		620	100	18	[66]
	SiNP-C	Magnetron sputtering	200	1900	200	86	[67]
Si NWs	SiNW/C	SFLS	2000	1200	1000	90	[68]
	SiNW/SiO_2	Metal-assisted chemical etching	200	2279	50	83	[69]
	SiNW	Mg reduction	500	1826.8	50	88.1	[70]
	SiNW/PEDOT[a)]	VLS	840	2510	100	80	[71]
	SiNW	CVD	420	321	650	100	[72]
	SiNW@G-CNT	CVD	420	1000	100	50	[73]
	SiNW/C	Lithography	300	1450	50	98	[74]
Si NSs	SiNS/C	$CaSi_2$ exfoliation	–	1450	10	76	[75]
	SiNS/SiO_x	$CaSi_2$ exfoliation	1000	647	50	81	[76]
	SiNS/C	Mg + NaCl reduction	1000	865	500	92.3	[38]
	SiNS	Mg reduction	100	900	100	40	[39]
	SiNS/G	Mg reduction	500	1500	50	60	[77]
	SiNS/C	Mg reduction	4000	1072	500	100	[78]
	SiNS	DC[b)] arc discharge	100	441	40	22	[79]
	SiNS	Hard template	0.1C	600	100	15	[80]
pSi	pSi/CNTs	Mg reduction	C/2	1500	500	80	[43]
	C@pSi@GF	CVD + Mg reduction	1000	969	200	81	[81]
	pSi nanotube	Hard template	C/20	1670	30	54	[82]
	pSi	Hard template	1C	2100	100	80	[83]
	pSi/C	Electrochemical etching	1	750	1000	80	[84]
	pSi/C	Solution method	2000	847	320	90	[85]
	pSi	Solution method	1000	851	350	69	[86]
	pSi@C	Mg reduction	0.2C	1257	200	87.5	[87]
	pSi@C	Mg reduction	200	1552	200	≈100	[88]
	pSi	Hard template	0.1C	1800	400	≈99	[89]
	pSi	Bi dealloying	1C	2100	100	84	[90]
	pSi@C	Mg reduction	50	N	30	N	[91]
	pSi@C	Mg reduction	500	1790	100	96	[92]
	pSi@C	Mg reduction	C/2	705	500	25.5	[93]
	pSi@C	Mg reduction	200	900	300	85.5	[94]

[a)]PEDOT: Poly (3,4-ethylenedioxythiophene). [b)]DC: Direct current.

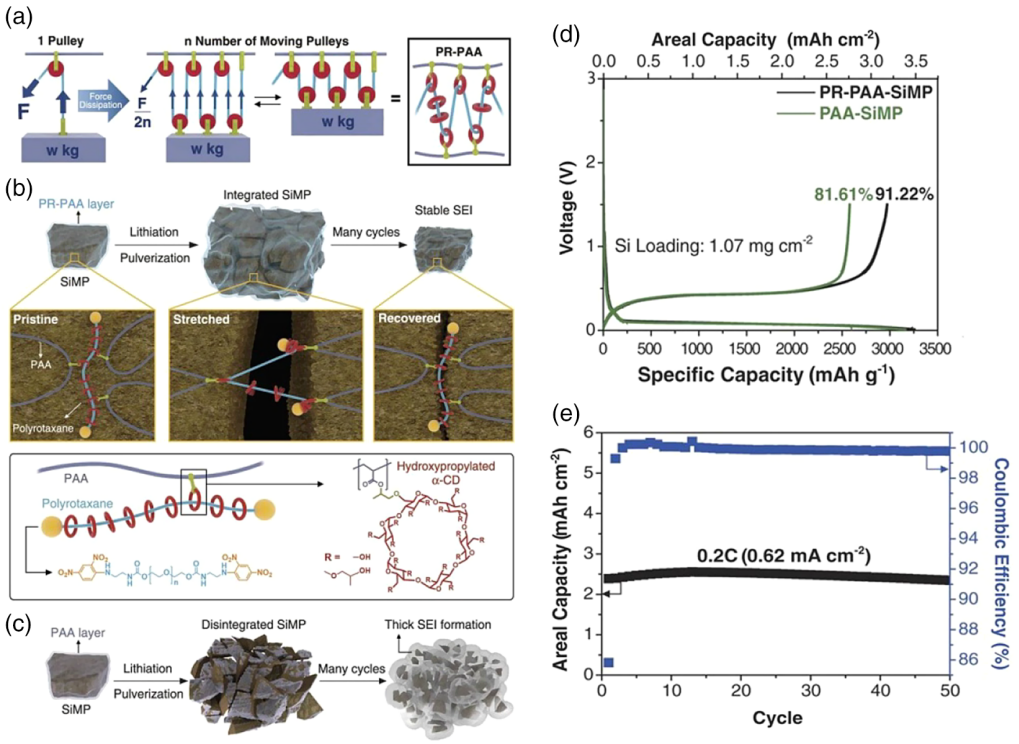

Figure 12. a) The pulley principle to lower the force in lifting an object. b) Graphical representation of the operation of polyrotaxane (PR)-PAA binder to dissipate the stress during repeated volume changes in Si microparticles (SiMPs), together with chemical structures of polyrotaxane and PAA. c) Schematic illustration of the pulverization of the PAA–SiMP electrode during cycling and its consequent SEI layer growth. d) The initial charge–discharge profiles of the PR-PAA–SiMP and PAA-SiMP electrodes when measured at 0.033 °C (100 mA g^{-1}). e) Cycling performance at 0.2 °C, along with coulombic efficiencies. Reproduced with permission.[95] Copyright 2017, American Association for the Advancement of Science.

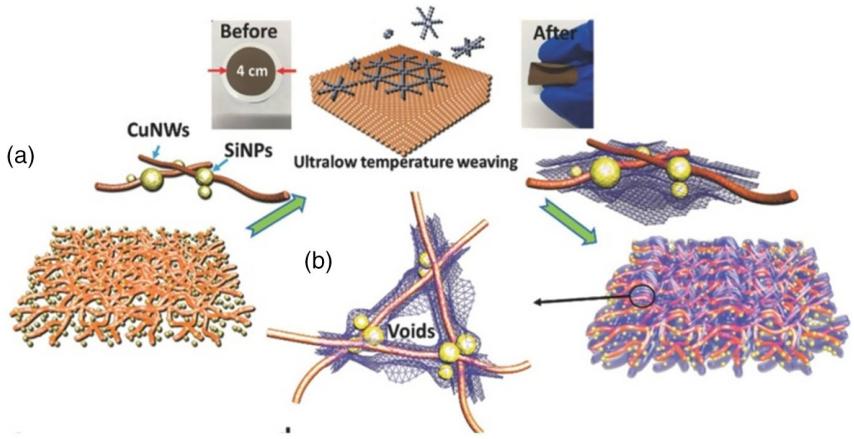

Figure 13. a) Schematic illustrations showing the processes for in situ weaving of the network of ultrathin graphdiyne (GDY) nanosheets on the Si anode (insets are the photos of electrodes with and without weaving GDY nanosheets); b) the possible structure showing the interactions among the ultrathin graphdiyne, SiNPs, and CuNWs and the reasonable voids for swallowing the volumetric increase. Reproduced with permission.[96] Copyright 2019, Elsevier.

Although the VLS growth mechanism can be used to prepare regular Si NW arrays, and this method has practical application prospects, the only drawback is that it is difficult to obtain a large number of 1D NW materials on the substrate (probably only ≈200–250 μg cm^{-2} or ≈0.75 mg h^{-1}). Moreover, if it is desired to fabricate an electrode by a conventional method of coating a slurry, it is necessary to peel the NW from the substrate by ultrasonic treatment, and in all probability, such a process will damage the NWs. Chan et al.[101] used the SFLS growth technique to prepare Si NWs (>45 mg h^{-1}) with large

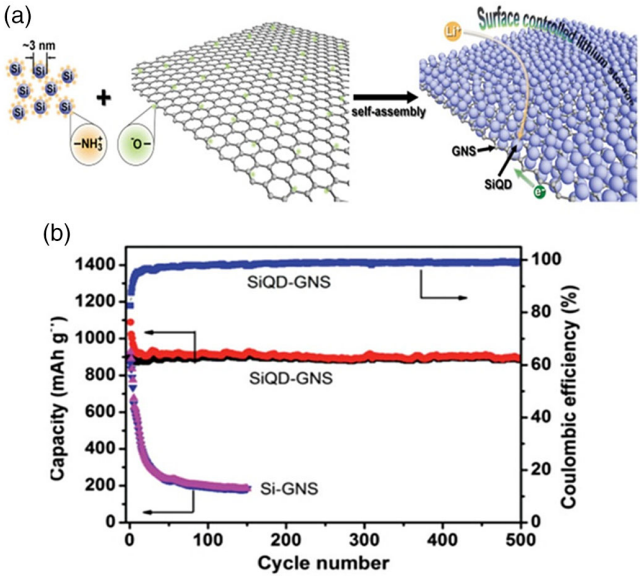

Figure 14. a) Schematic illustration of the synthesis of SiQD–GNS. An electrostatic self-assembly strategy enables the facile and controllable synthesis of GNS-supported uniform ultrasmall Si QDs featuring unprecedented surface-controlled lithium storage behavior; b) cycling performances at 2 A g^{-1}. All the specific capacities calculated and current rates used are based on the total weight of respective active materials in the electrodes. Reproduced with permission.[8] Copyright 2015, Wiley-VCH.

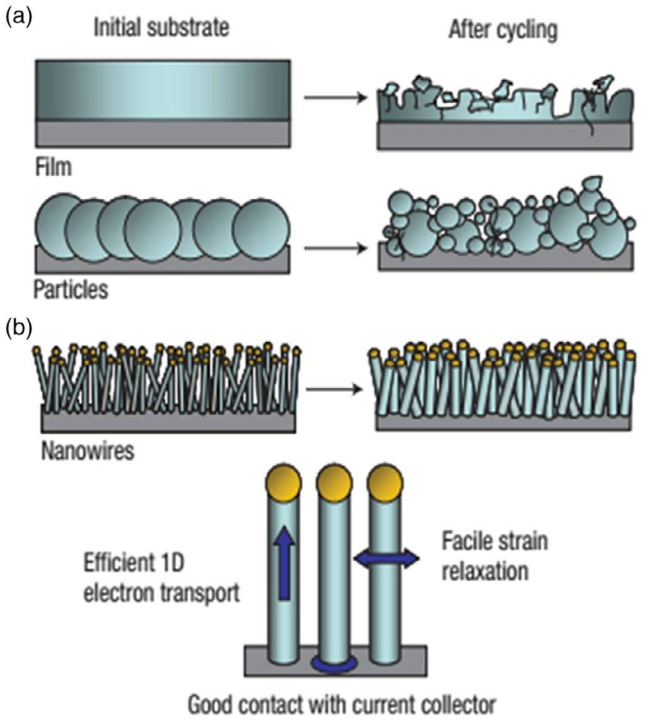

Figure 15. The scheme of morphological changes that occur in Si during electrochemical cycling. a) The volume of silicon anodes changes by about 400% during cycling. As a result, Si films and particles tend to pulverize during cycling. Much of the material loses contact with the current collector, resulting in poor transport of electrons, as indicated by the arrow. b) NWs grown directly on the current collector do not pulverize or break into smaller particles after cycling. Rather, facile strain relaxation in the NWs allows them to increase in diameter and length without breaking. This NW anode design has each NW connecting with the current collector, allowing for efficient 1D electron transport down the length of every NW. Reproduced with permission.[99] Copyright 2008, Springer Nature Publishing AG.

scale in solution. The obtained Si NWs can be prepared by a conventional slurry coating method. After coating a layer of multiwalled carbon nanotubes (MWNTs) on the surface of the Si NW, the obtained SiNW/MWNT composite exhibits high capacity and good cycle stability, and the reversible capacity after charging and discharging for 30 cycles still has 1500 mA h g^{-1}.

4.2.3. 2D and 3D Si Nanosheets and Porous Si

If the Si wafer is thin enough, the electrochemical performance should be similar to that of the NWs. However, due to the limited preparation methods, few literatures on the preparation of ultrathin Si nanosheets have been reported so far. Although stripping of $CaSi_2$ in a strong acid system at −30 °C can obtain surface-atomized H-passivated Si nanosheets with several atomic layers, the Si_6H_6 material is used as a negative electrode material for lithium batteries, and its interaction with Li is limited to the exchange of H and Li on the surface of Si wafers, resulting in low capacity. For example, Kumai et al.[75] used Si_6H_6 as a negative electrode for lithium batteries by pyrolysis of a layer of carbon and investigated the electrochemical properties of the materials at different heat treatment temperatures. The results were found to be unsatisfactory, and the capacity was degraded to 60% after only ten cycles. $CaSi_2$ was also used as a precursor by our group to produce partially oxidizing SiO_x nanosheets. The commercially available $CaSi_2$ was solvothermally treated at 190 °C for 3 days in the presence of ionic liquid (IL) butyl-3-methylimidazolium chloride and NH_4Cl. The layers of $CaSi_2$ were unfolded by cationic intercalation (e.g., H^+ produced via the decomposition of NH_4Cl at a high temperature). Because of the inherent instability of the free-standing silicon nanosheet, it was partly oxidized to form ultrathin SiO_x nanosheets. To separate the SiO_x nanosheets from the contaminated crystalline Si particles, the obtained products were sonicated in acetonitrile for several hours. After removing the dark metallic precipitates of Si, the yellow SiO_x nanosheets were collected from the upper dispersion. The SiO_x nanosheets after coating with carbon exhibited excellent cycling and good rate performance when used as anode materials in LIBs. Even after charging–discharging for 400 cycles, no significant capacity decay was observed. This method features convenient high-yield synthesis of ultrathin SiO_x nanosheets, which served as promising candidates for practical high-energy-density LIB applications. The scanning electron microscopy (SEM) and transmission electron microscopy (TEM) characterizations and scheme and battery testing results are shown in **Figure 16**.

The templating method is also another method commonly used to prepare Si sheets. Lu et al.[101] utilized graphene oxide

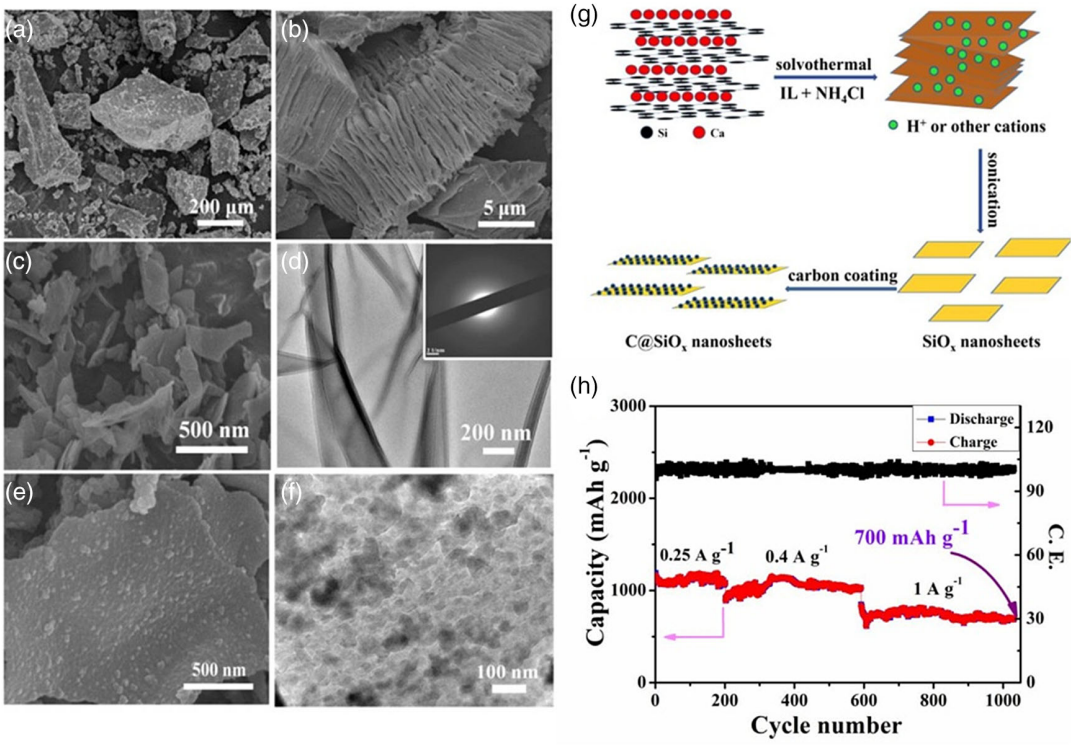

Figure 16. SEM images of a) $CaSi_2$. b) $CaSi_2$ after solvothermal treatment for three days and c) SiO_x nanosheets. d) TEM image of SiO_x nanosheets (the inset shows the corresponding ED pattern). e) SEM image of SiO_x@C nanocomposites. f) TEM image of SiO_x@C nanocomposites. g) A schematic illustration of the preparation of the SiO_x@C nanosheets. h) Cycling performance of SiO_x@C nanocomposite anode at various current densities. Reproduced with permission.[37] Copyright 2016, Royal Society of Chemistry.

(GO) as a hard template. First, a layer of SiO_2 gel was coated on the surface of ultrathin GO nanosheets and calcined in air to remove GO to obtain SiO_2 nanosheet precursor. The Si nanosheets were then obtained by magnesium thermal reduction. This method enables the preparation of Si nanosheets of different sizes by adjusting the size of GO, and the resulting Si wafer has a thickness of about 3.5 nm. The Si nanosheet was used as the negative electrode of LIBs. Compared with the Si NPs with a particle size of about 50 nm, the cycle performance is slightly better, but there is still a big gap from the practical application. Therefore, pure Si nanosheets do not exhibit excellent electrochemical performance as Si NWs. However, it is worth considering that Si films with good crystallinity are advantageous compared with Si NP-based anodes as in films the free volume between NPs is eliminated, resulting in very high volumetric energy density. However, Si undergoes volume expansion (contraction) under lithiation (delithiation) of up to 300%. This large volume expansion leads to stress build-up at the interface between the Si film and the current collector, leading to delamination of Si from the surface of the current collector.[102]

Because of the abundant pore structures, pSi can greatly reduce the destructive effect on the active material structure due to volume change during charge and discharge.[81–83,87,89] Recently, some pSi materials can be obtained by the templating and etching methods and show good electrochemical performance.[103] Our group recently also developed a simple, facile solution-based method to prepare amorphous PSi via room-temperature reaction of Mg_2Si with $HSiCl_3$ in CH_2Cl_2 for merely several hours in the presence of amines, as shown in **Figure 17**. The carbon-coated PSi nanocomposite exhibited excellent electrochemical properties when served as anodes for LIBs. It delivered a specific discharge capacity of about 847 mA h g^{-1} over 320 cycles at a high current density of 2 A g^{-1}, with a capacity retention of 90%. This new solution preparative method allows facile, high-yield, and large-scale production of pSi without using extremely reactive precursors and harsh conditions, superior to the conventional methods including etching of bulk Si, CVD of silane or $SiCl_4$, magnesiothermic reduction of SiO_2, reduction of $SiCl_4$, and oxidation of NaSi. It provides a convenient way for the massive production of pSi for use in LiBs, drug delivery systems, catalysis, etc.[85]

In addition, it should be noted that the functionalization of silicon surface will have a significant impact on electrochemical performance. It has been found that for silicon-based negative materials, the binders with carboxyl groups, such as sodium alginate (SA), sodium carboxymethyl cellulose (CMC), PAA, or partially lithium PAA, are more helpful to improve the performance.[104] On this foundation, Bie et Al. developed a robust Si electrode via prepolymerizing dopamine on the Si particle surface.[105]

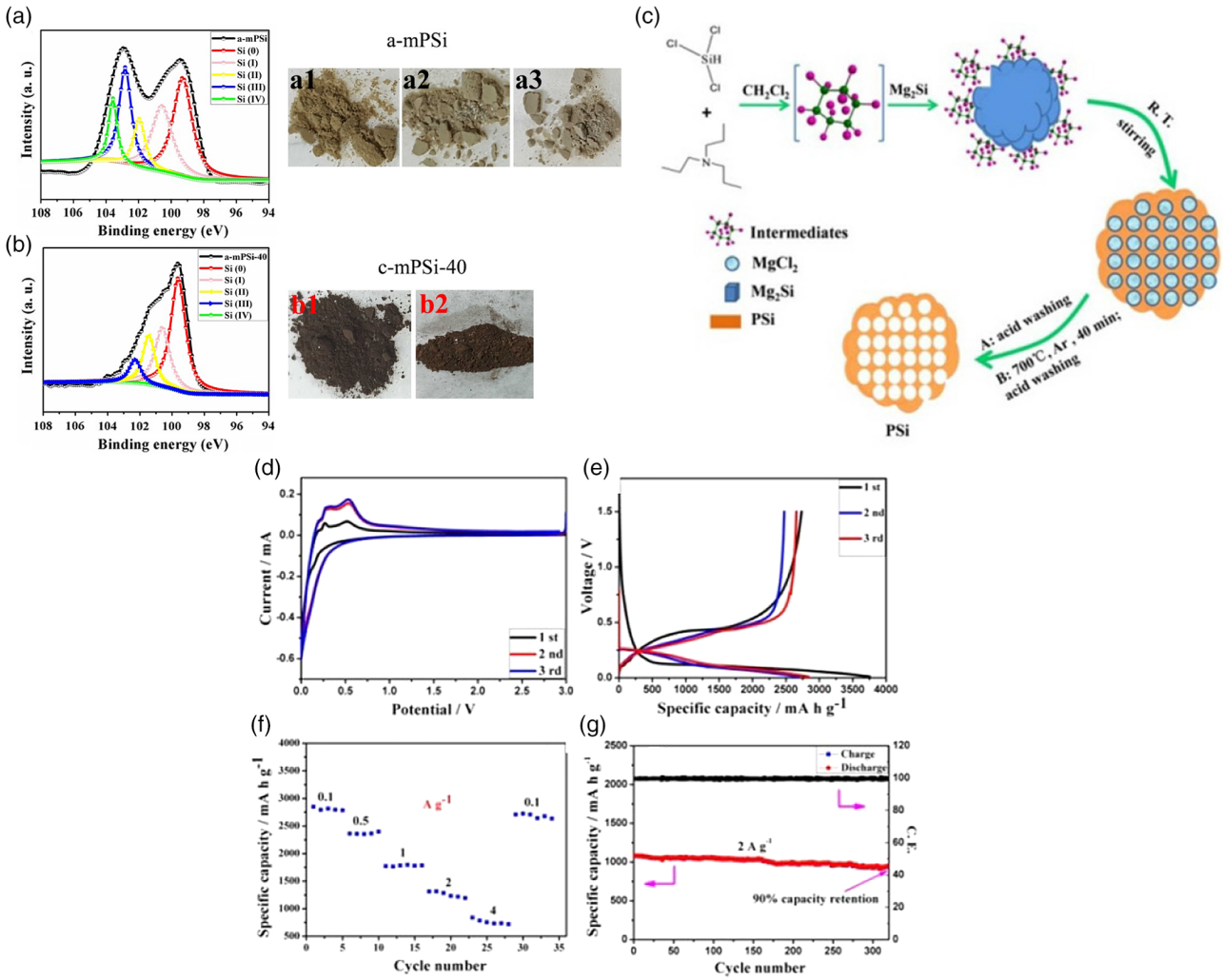

Figure 17. a) Si 2p X-ray photoelectron spectroscopy (XPS) spectra of a-mPSi (a1, a2, and a3 show the digital photos of a-mPSi after being exposed in air for 1, 12, and 24 h, respectively) and b) c-mPSi-40 (b1 and b2 show the digital photos of c-mPSi-40 after being exposed in air for 1 and 48 h). The red, pink, yellow, blue, and green lines are deconvoluted peaks for Si^0, Si^{1+}, Si^{2+}, Si^{3+}, and Si^{4+}, respectively. c) Schematic illustration for preparing mPSi. d) Cyclic voltammetry (CV) curves of the c-mPSi-40@C electrode. e) Voltage profiles of the c-mPSi-40@C electrode. f) Rate performance of the c-mPSi-40@C electrode cycled at different current densities. g) Long-term cycling stability of the c-mPSi-40@C electrode cycled at 2 A g^{-1}. Reproduced with permission.[85] Copyright 2017, American Chemical Society.

5. Conclusion and Outlook

In short, in the field of high-energy-density lithium batteries, silicon-based nanomaterials replace commercial carbon materials as anodes with high specific capacity (≈4200 mAh g^{-1}, about 11 times that of carbon materials), low operating potential (<0.5 V vs Li/Li^+), abundant silicon sources (the second highest in the crust), and low potential cost and have received widespread attention. However, the actual use of silicon-based anode materials still has a very big problem. The main reason is that the silicon-based anode material has a very large volume change during battery charge and discharge (300%–400% volume change), which causes the pulverization of the electrode and the unstability of the SEI film, resulting in poor cycling performance of batteries. Therefore, improving the electrochemical performance of silicon-based anodic batteries, especially the cycle stability, is still an urgent issue to be addressed. In addition, although silicon is abundant in the Earth's crust, the cost of nanosilicon materials currently on the market is still very high due to the limited synthesis method. At present, the commercial method for preparing nanosilicon is generally by high-temperature CVD, but this inevitably increases the cost of synthesis. Therefore, the development of low-cost and facile synthetic pathways to prepare silicon-based nanomaterials with unique structures is also a very important scientific and technical issue.

The future research and development trends of Si materials for LIB applications should be based on the following aspects: 1) Developing new, simple, and cost-effective ways to controllably prepare nano-structured Si materials and greatly reduce the cost of preparing Si nanomaterials is required. 2) The Rational design and preparation of Si and Si-based hybrids for use as anodes in LIBs is required. On the basis of deeply understanding the

structure activity relationships of various Si structures, it is possible to investigate the lithium storage mechanism of Si by using some in situ characterizations.3) The safety of such anodic batteries must be taken seriously, how to build a better battery with reliable safety is necessary to be emphasized on.

Acknowledgements

This work was supported by the Research Fund of the Natural Science Foundation of Jiangsu Province (No. BK20181056), Industry Universities Research Cooperation Project of Jiangsu Province (2018), Funding for school-level research projects of Yancheng Institute of Technology, State Key Laboratory of Coordination Chemistry (No. SKLCC1802), Joint Open of Jiangsu Collaborative Innovation Center for Ecological Building Material and Environmental Protection Equipments, and Key Laboratory for Advanced Technology in Environmental Protection of Jiangsu Province (No. JH201844).

Conflict of Interest

The authors declare no conflict of interest.

Keywords

anodes, energy storage, lithium-ion batteries, silicon nanostructures, synthesis methods

Received: August 12, 2019
Revised: September 5, 2019
Published online: September 25, 2019

[1] Y. Oh, C. Choi, D. Hong, S. D. Kong, S. Jin, *Nano Lett.* **2012**, *12*, 2045.
[2] M. E. Davis, *Nature* **2002**, *417*, 813.
[3] a) B. Tian, X. Zheng, T. J. Kempa, Y. Fang, N. Yu, G. Yu, J. Huang, C. M. Lieber, *Nature* **2007**, *449*, 885; b) M. T. Bjork, H. Schmid, J. Knoch, H. Riel, W. Riess, *Nat. Nanotechnol.* **2009**, *4*, 103.
[4] a) W. Zhang, M. Hu, X. Liu, Y. Wei, N. Li, Y. Qin, *J. Alloy. Compd.* **2016**, *679*, 391; b) A. A. Ensafi, F. Rezaloo, B. Rezaei, *Sens. Actuators, B* **2016**, *231*, 239; c) M. Boccard, Z. C. Holman, *J. Appl. Phys.* **2015**, *118*, 065704.
[5] Q. Li, Y. He, J. Chang, L. Wang, H. Chen, Y. W. Tan, H. Wang, Z. Shao, *J. Am. Chem. Soc.* **2013**, *135*, 14924.
[6] Q. Li, T. Y. Luo, M. Zhou, H. Abroshan, J. Huang, H. J. Kim, N. L. Rosi, Z. Shao, R. Jin, *ACS Nano* **2016**, *10*, 8385.
[7] a) J. H. Park, L. Gu, G. von Maltzahn, E. Ruoslahti, S. N. Bhatia, M. J. Sailor, *Nat. Mater.* **2009**, *8*, 331; b) J. H. Warner, A. Hoshino, K. Yamamoto, R. D. Tilley, *Angew. Chem., Int. Ed.* **2005**, *44*, 4550; c) F. Erogbogbo, K.-T. Yong, I. Roy, G. Xu, P. N. Prasad, M. T. Swihart, *ACS Nano* **2008**, *2*, 6.
[8] B. Wang, X. Li, B. Luo, L. Hao, M. Zhou, X. Zhang, Z. Fan, L. Zhi, *Adv. Mater.* **2015**, *27*, 1526.
[9] a) X. Cheng, E. Hinde, D. M. Owen, S. B. Lowe, P. J. Reece, K. Gaus, J. J. Gooding, *Adv. Mater.* **2015**, *27*, 6144; b) K. Linehan, H. Doyle, *Small* **2014**, *10*, 584; c) R. K. Baldwin, K. A. Pettigrew, E. Ratai, M. P. Augustine, S. M. Kauzlarich, *Chem. Commun.* **2002**, *17*, 1822; d) S. Walia, A. Guliani, A. Acharya, *ACS Sustainable Chem. Eng.* **2017**, *5*, 1425; e) B. F. P. McVey, S. Prabakar, J. J. Gooding, R. D. Tilley, *ChemPlusChem* **2017**, *82*, 60; f) B. Sharma, S. Tanwar, T. Sen, *ACS Sustainable Chem. Eng.* **2019**, *7*, 3309; g) X. Geng, Z. Li, Y. Hu, H. Liu, Y. Sun, H. Meng, Y. Wang, L. Qu, Y. Lin, *ACS Appl. Mater. Interfaces* **2018**, *10*, 27979; h) Y. Han, Y. Chen, J. Feng, J. Liu, S. Ma, X. Chen, *Anal. Chem.* **2017**, *89*, 3001.
[10] T. K. Purkait, M. Iqbal, M. A. Islam, M. H. Mobarok, C. M. Gonzalez, L. Hadidi, J. G. Veinot, *J. Am. Chem. Soc.* **2016**, *138*, 7114.
[11] J. R. Heath, *Science* **1992**, *258*, 1131.
[12] B. F. P. McVey, R. D. Tilley, *Acc. Chem. Res.* **2014**, *47*, 3045.
[13] a) C.-S. Yang, R. A. Bley, S. M. Kauzlarich, H. W. H. Lee, G. R. Delgado, *J. Am. Chem. Soc.* **1999**, *121*, 5191; b) C.-W. Hsu, D. Septiadi, C.-H. Lai, P. Chen, P. H. Seeberger, L. De Cola, *ChemPlusChem* **2017**, *82*, 660.
[14] a) M. Batmunkh, M. Myekhlai, A. S. R. Bati, S. Sahlos, A. D. Slattery, T. M. Benedetti, V. R. Gonçales, C. T. Gibson, J. J. Gooding, R. D. Tilley, J. G. Shapter, *J. Mater. Chem. A* **2019**, *7*, 12974; b) J.-S. Tsai, K. Dehvari, W.-C. Ho, K. Waki, J.-Y. Chang, *Adv. Mater. Interfaces* **2019**, *6*, 1801745.
[15] H.-L. Ye, S.-J. Cai, S. Li, X.-W. He, W.-Y. Li, Y.-H. Li, Y.-K. Zhang, *Anal. Chem.* **2016**, *88*, 11631.
[16] a) Z. Li, X. Ren, C. Hao, X. Meng, Z. Li, *Sens. Actuators, B* **2018**, *260*, 426; b) W. Jeong, S. Jo, J. Park, B. Kwon, Y. Choi, A. Chae, S. Y. Park, I. In, *J. Mater. Sci.* **2018**, *53*, 2443; c) X. Zheng, D. Zhang, Z. Fan, Z. Huang, H. Mao, Y. Ma, *J. Mater. Sci.* **2019**, *54*, 9707.
[17] R. K. Grötsch, A. Angı, Y. G. Mideksa, C. Wanzke, M. Tena-Solsona, M. J. Feige, B. Rieger, J. Boekhoven, *Angew. Chem., Int. Ed.* **2018**, *57*, 14608.
[18] S. Kano, Y. Tada, S. Matsuda, M. Fujii, *ACS Appl. Mater. Interfaces* **2018**, *10*, 20672.
[19] a) C. M. Hessel, D. Reid, M. G. Panthani, M. R. Rasch, B. W. Goodfellow, J. Wei, H. Fujii, V. Akhavan, B. A. Korgel, *Chem. Mater.* **2012**, *24*, 393; b) D. S. English, L. E. Pell, Z. Yu, P. F. Barbara, B. A. Korgel, *Nano Lett.* **2002**, *2*, 681; c) J. D. Holmes, K. J. Ziegler, R. C. Doty, L. E. Pell, K. P. Johnston, B. A. Korgel, *J. Am. Chem. Soc.* **2001**, *123*, 3743.
[20] a) G. Viera, S. Huet, M. Mikikian, L. Boufendi, *Thin Solid Films* **2002**, *403–404*, 467; b) G. Viera, M. Mikikian, E. Bertran, P. R. i. Cabarrocas, L. Boufendi, *J. Appl. Phys.* **2002**, *92*, 4684; c) M. Fujii, H. Sugimoto, S. Kano, *Chem. Commun.* **2018**, *54*, 4375.
[21] a) Z. Chen, Y. Wang, H. He, Y. Zou, J. Wang, Y. Li, *Solid State Commun.* **2005**, *135*, 247; b) H. Adhikari, P. C. McIntyre, S. Sun, P. Pianetta, C. E. D. Chidsey, *Appl. Phys. Lett.* **2005**, *87*, 263109; c) Y. Cui, Z. Zhong, D. Wang, W. U. Wang, C. M. Lieber, *Nano Lett.* **2003**, *3*, 149.
[22] R. S. Wagner, W. C. Ellis, *Appl. Phys. Lett.* **1964**, *4*, 89.
[23] N. Ferralis, R. Maboudian, C. Carraro, *J. Am. Chem. Soc.* **2008**, *130*, 2681.
[24] a) V. Schmidt, J. V. Wittemann, U. Gösele, *Chem. Rev.* **2010**, *110*, 361; b) V. Schmidt, J. V. Wittemann, S. Senz, U. Gösele, *Adv. Mater.* **2009**, *21*, 2681; c) C. M. Lieber, *MRS Bull.* **2003**, *28*, 486.
[25] a) E. C. Garnett, W. Liang, P. Yang, *Adv. Mater.* **2007**, *19*, 2946; b) H.-Y. Tuan, D. C. Lee, B. A. Korgel, *Angew. Chem., Int. Ed.* **2006**, *45*, 5184.
[26] Y. Wu, Y. Cui, L. Huynh, C. J. Barrelet, D. C. Bell, C. M. Lieber, *Nano Lett.* **2004**, *4*, 433.
[27] W. I. Park, G. Zheng, X. Jiang, B. Tian, C. M. Lieber, *Nano Lett.* **2008**, *8*, 3004.
[28] a) N. Fukata, T. Oshima, T. Tsurui, S. Ito, K. Murakami, *Sci. Technol. Adv. Mater.* **2016**, *6*, 628; b) J. B. Hannon, S. Kodambaka, F. M. Ross, R. M. Tromp, *Nature* **2006**, *440*, 69; c) J. B. Chang, J. Z. Liu, P. X. Yan, L. F. Bai, Z. J. Yan, X. M. Yuan, Q. Yang, *Mater. Lett.* **2006**, *60*, 2125; d) Y. Wang, V. Schmidt, S. Senz, U. Gosele, *Nat. Nanotechnol.* **2006**, *1*, 186; e) S. Q. Feng, D. P. Yu, H. Z. Zhang, Z. G. Bai, Y. Ding, *J. Cryst. Growth* **2000**, *209*, 513.
[29] J. D. Holmes, K. P. Johnston, R. C. Doty, B. A. Korgel, *Science* **2000**, *287*, 1471.

[30] A. T. Heitsch, D. D. Fanfair, H.-Y. Tuan, B. A. Korgel, *J. Am. Chem. Soc.* **2008**, *130*, 5436.
[31] R. Venkatesan, M. K. Arivalagan, V. Venkatachalapathy, J. M. Pearce, J. Mayandi, *Mater. Lett.* **2018**, *221*, 206.
[32] B. M. Rey, R. Elnathan, R. Ditcovski, K. Geisel, M. Zanini, M.-A. Fernandez-Rodriguez, V. V. Naik, A. Frutiger, W. Richtering, T. Ellenbogen, N. H. Voelcker, L. Isa, *Nano Lett.* **2016**, *16*, 157.
[33] a) Z. Liu, K. Xu, P. She, S. Yin, X. Zhu, H. Sun, *Chem. Sci.* **2016**, *7*, 1926; b) X. Chen, A. R. McDonald, *Adv. Mater.* **2016**, *28*, 5738; c) L. Fei, S. Lei, W. B. Zhang, W. Lu, Z. Lin, C. H. Lam, Y. Chai, Y. Wang, *Nat. Commun.* **2016**, *7*, 12206; d) A. Achari, S. Sahana, M. Eswaramoorthy, *Energy Environ. Sci.* **2016**, *9*, 1224; e) H. Tang, J. Wang, H. Yin, H. Zhao, D. Wang, Z. Tang, *Adv. Mater.* **2015**, *27*, 1117; f) K. Huang, G. Liu, Y. Lou, Z. Dong, J. Shen, W. Jin, *Angew. Chem., Int. Ed.* **2014**, *53*, 6929; g) W. Wei, H. Liang, K. Parvez, X. Zhuang, X. Feng, K. Mullen, *Angew. Chem., Int. Ed.* **2014**, *53*, 1570.
[34] U. Kim, I. Kim, Y. Park, K.-Y. Lee, S.-Y. Yim, J.-G. Park, H.-G. Ahn, S.-H. Park, H.-J. Choi, *ACS Nano* **2011**, *5*, 2176.
[35] S. Yamanaka, H. Matsu-ura, M. Ishikawa, *Mater. Res. Bull.* **1996**, *31*, 307.
[36] a) H. Nakano, M. Nakano, K. Nakanishi, D. Tanaka, Y. Sugiyama, T. Ikuno, H. Okamoto, T. Ohta, *J. Am. Chem. Soc.* **2012**, *134*, 5452; b) H. Okamoto, Y. Sugiyama, K. Nakanishi, T. Ohta, T. Mitsuoka, H. Nakano, *Chem. Mater.* **2015**, *27*, 1292; c) A. Molle, C. Grazianetti, L. Tao, D. Taneja, M. H. Alam, D. Akinwande, *Chem. Soc. Rev.* **2018**, *47*, 6370; d) H. Itahara, X. Wu, H. Imagawa, S. Yin, K. Kojima, S. F. Chichibu, T. Sato, *Dalton Trans.* **2017**, *46*, 8643.
[37] L. Sun, T. Su, L. Xu, M. Liu, H. B. Du, *Chem. Commun.* **2016**, *52*, 4341.
[38] J. Ryu, D. Hong, S. Choi, S. Park, *ACS Nano* **2016**, *10*, 2843.
[39] X.-Y. Yue, A. Abulikemu, X.-L. Li, Q.-Q. Qiu, F. Wang, X.-J. Wu, Y.-N. Zhou, *J. Power Sources* **2019**, *410–411*, 132.
[40] a) X. Li, B. Huang, C. Qiu, Z. Li, L.-H. Shao, H. Liu, *J. Alloy. Compd.* **2016**, *681*, 109; b) M. Wu, Q. Tang, F. Dong, Y. Wang, D. Li, Q. Guo, Y. Liu, J. Qiao, *Phys. Chem. Chem. Phys.* **2016**, *18*, 18665; c) L. Nan, Z. Fan, W. Yue, Q. Dong, L. Zhu, L. Yang, L. Fan, *J. Mater. Chem.* **2016**, *4*, 8898; d) Y. Song, J. He, H. Wu, X. Li, J. Yu, Y. Zhang, L. Wang, *Electrochim. Acta* **2015**, *182*, 165; e) G.-L. Cao, Y.-M. Yan, T. Liu, D. Rooney, Y.-F. Guo, K.-N. Sun, *Carbon* **2015**, *94*, 680; f) K. Narasimharao, A. Al-Shehri, S. Al-Thabaiti, *Appl. Catal., A* **2015**, *505*, 431.
[41] a) B. Chang, Y. Tang, M. Liang, H. Jansen, F. Jensen, B. Wang, K. Mølhave, J. Hübner, H. Sun, *ChemNanoMat* **2019**, *5*, 92; b) N. Harpak, G. Davidi, D. Schneier, S. Menkin, E. Mados, D. Golodnitsky, E. Peled, F. Patolsky, *Nano Lett.* **2019**, *19*, 1944; c) K. Wang, S. Pei, Z. He, L.-a. Huang, S. Zhu, J. Guo, H. Shao, J. Wang, *Chem. Eng. J.* **2019**, *356*, 272; d) N. Kim, H. Park, N. Yoon, J. K. Lee, *ACS Nano* **2018**, *12*, 3853.
[42] X. Fan, X. Jiang, W. Wang, Z. Liu, *Mater. Lett.* **2016**, *180*, 109.
[43] W. Wang, Z. Favors, R. Ionescu, R. Ye, H. H. Bay, M. Ozkan, C. S. Ozkan, *Sci. Rep.* **2015**, *5*, 8781.
[44] F. Dai, J. Zai, R. Yi, M. L. Gordin, H. Sohn, S. Chen, D. Wang, *Nat. Commun.* **2014**, *5*, 3605.
[45] L. Lin, X. Xu, C. Chu, M. K. Majeed, J. Yang, *Angew. Chem., Int. Ed.* **2016**, *55*, 14063.
[46] M. F. Oszajca, M. I. Bodnarchuk, M. V. Kovalenko, *Chem. Mater.* **2014**, *26*, 5422.
[47] a) K. Huo, W. An, J. Fu, B. Gao, L. Wang, X. Peng, G. J. Cheng, P. K. Chu, *J. Power Sources* **2016**, *324*, 233; b) H. Ma, H. Jiang, Y. Jin, L. Dang, Q. Lu, F. Gao, *Carbon* **2016**, *105*, 586; c) M. Tian, W. Wang, Y. Liu, K. L. Jungjohann, C. Thomas Harris, Y.-C. Lee, R. Yang, *Nano Energy* **2015**, *11*, 500; d) K. Wang, S. Luo, Y. Wu, X. He, F. Zhao, J. Wang, K. Jiang, S. Fan, *Adv. Funct. Mater.* **2013**, *23*, 846; e) S. Chen, W. Yeoh, Q. Liu, G. Wang, *Carbon* **2012**, *50*, 4557; f) Y. Ito, M. Kawakubo, M. Ueno, H. Okuma, Q. Si, T. Kobayashi, K. Hanai, N. Imanishi, A. Hirano, M. B. Phillipps, Y. Takeda, O. Yamamoto, *J. Power Sources* **2012**, *214*, 84.
[48] a) C. Ma, J. Zhang, M. Xu, Q. Xia, J. Liu, S. Zhao, L. Chen, A. Pan, D. G. Ivey, W. Wei, *J. Power Sources* **2016**, *317*, 103; b) X. Du, Q. Wang, T. Feng, X. Chen, L. Li, L. Li, X. Meng, L. Xiong, X. Sun, L. Lu, Y. Xu, *Sci. Rep.* **2016**, *6*, 20138; c) S. Mohapatra, S. V. Nair, D. Santhanagopalan, A. K. Rai, *Electrochim. Acta* **2016**, *206*, 217; d) X. Ma, N. Wang, Y. Qian, Z. Bai, *Mater. Lett.* **2016**, *168*, 5; e) Y. Feng, H. Zhang, Y. Zhang, Y. Bai, Y. Wang, *J. Mater. Chem. A* **2016**, *4*, 3267; f) X. H. Huang, J. B. Wu, Y. Lin, R. Q. Guo, *Mater. Lett.* **2016**, *175*, 199; g) Q. Liu, Y. Dou, B. Ruan, Z. Sun, S.-L. Chou, S. X. Dou, *Chem. Eur. J.* **2016**, *22*, 5853; h) X. Fan, S. Li, H. Zhou, L. Lu, *Electrochim. Acta* **2015**, *180*, 1041; i) Z. Fan, J. Liang, W. Yu, S. Ding, S. Cheng, G. Yang, Y. Wang, Y. Xi, K. Xi, R. V. Kumar, *Nano Energy* **2015**, *16*, 152; j) S. H. Park, W. J. Lee, *Sci. Rep.* **2015**, *5*, 9754; k) X.-H. Ma, S.-S. Zeng, B.-K. Zou, X. Liang, J.-Y. Liao, C.-H. Chen, *RSC Adv.* **2015**, *5*, 57300.
[49] a) C. Yue, Y. Yu, Z. Wu, S. Sun, X. He, J. Li, L. Zhao, S. Wu, J. Li, J. Kang, L. Lin, *ACS Appl. Mater. Interfaces* **2016**, *8*, 7806; b) J. Wu, Z. Zhu, H. Zhang, H. Fu, H. Li, A. Wang, H. Zhang, *Sci. Rep.* **2016**, *6*, 29356; c) K. Feng, W. Ahn, G. Lui, H. W. Park, A. G. Kashkooli, G. Jiang, X. Wang, X. Xiao, Z. Chen, *Nano Energy* **2016**, *19*, 187; d) N. Qaiser, Y. J. Kim, C. S. Hong, S. M. Han, *J. Phys. Chem. C* **2016**, *120*, 6953; e) J. Hwang, C. Jo, M. G. Kim, J. Chun, E. Lim, S. Kim, S. Jeong, Y. Kim, J. Lee, *ACS Nano* **2015**, *9*, 5299; f) X. Liu, J. Hao, X. Liu, C. Chi, N. Li, F. Endres, Y. Zhang, Y. Li, J. Zhao, *Chem. Commun.* **2015**, *51*, 2064; g) J. Qin, C. He, N. Zhao, Z. Wang, C. Shi, E.-Z. Liu, J. Li, *ACS Nano* **2014**, *8*, 1728.
[50] J. Liu, X. Chen, J. Kim, Q. Zheng, H. Ning, P. Sun, X. Huang, J. Liu, J. Niu, P. V. Braun, *Nano Lett.* **2016**, *16*, 4501.
[51] a) L. Oakes, A. Westover, J. W. Mares, S. Chatterjee, W. R. Erwin, R. Bardhan, S. M. Weiss, C. L. Pint, *Sci. Rep.* **2013**, *3*, 3020; b) H. Wu, G. Yu, L. Pan, N. Liu, M. T. McDowell, Z. Bao, Y. Cui, *Nat. Commun.* **2013**, *4*, 1943; c) S. E. Rowlands, R. J. Latham, W. S. Schlindwein, *Ionics* **1999**, *5*, 144.
[52] J. Rohrer, K. Albe, *J. Phys. Chem. C* **2013**, *117*, 18796.
[53] B. M. Bang, J.-I. Lee, H. Kim, J. Cho, S. Park, *Adv. Energy Mater.* **2012**, *2*, 878.
[54] L. Yue, S. Wang, X. Zhao, L. Zhang, *J. Mater. Chem.* **2012**, *22*, 1094.
[55] L. Pan, H. Wang, D. Gao, S. Chen, L. Tan, L. Li, *Chem. Commun.* **2014**, *50*, 5878.
[56] P. Gu, R. Cai, Y. Zhou, Z. Shao, *Electrochim. Acta* **2010**, *55*, 3876.
[57] Y. Tian, Y. An, J. Feng, *ACS Appl. Mater. Interfaces* **2019**, *11*, 10004.
[58] K. Xu, Z. Zhang, W. Su, Z. Wei, G. Zhong, C. Wang, X. Huang, *Funct. Mater. Lett.* **2016**, *10*, 1650073.
[59] L. Sun, T. Su, L. Xu, H.-B. Du, *Phys. Chem. Chem. Phys.* **2016**, *18*, 1521.
[60] B. Li, S. Yang, S. Li, B. Wang, J. Liu, *Adv. Energy Mater.* **2015**, *5*, 1500289.
[61] X. Feng, J. Yang, Q. Lu, J. Wang, Y. Nuli, *Phys. Chem. Chem. Phys.* **2013**, *15*, 14420.
[62] J. Y. Howe, D. J. Burton, Y. Qi, H. M. Meyer, M. Nazri, G. A. Nazri, A. C. Palmer, P. D. Lake, *J. Power Sources* **2013**, *221*, 455.
[63] J. Zhou, Y. Hu, X. Li, C. Wang, L. Zuin, *RSC Adv.* **2014**, *4*, 20226.
[64] A. Magasinski, P. Dixon, B. Hertzberg, A. Kvit, J. Ayala, G. Yushin, *Nat. Mater.* **2010**, *9*, 353.
[65] I. Kang, J. Jang, K.-W. Yi, Y. W. Cho, *J. Alloys Compd.* **2019**, *770*, 369.
[66] U. Tocoglu, O. Cevher, M. O. Guler, H. Akbulut, *Appl. Surf. Sci.* **2014**, *305*, 402.

[67] Y. Tong, Z. Xu, C. Liu, G. a. Zhang, J. Wang, Z. G. Wu, *J. Power Sources* **2014**, *247*, 78.
[68] T. D. Bogart, D. Oka, X. Lu, M. Gu, C. Wang, B. A. Korgel, *ACS Nano* **2014**, *8*, 915.
[69] S. Sim, P. Oh, S. Park, J. Cho, *Adv. Mater.* **2013**, *25*, 4498.
[70] J. Chen, L. Yang, S. Rousidan, S. Fang, Z. Zhang, S. Hirano, *Nanoscale* **2013**, *5*, 10623.
[71] Y. Yao, N. Liu, M. T. McDowell, M. Pasta, Y. Cui, *Energy Environ. Sci.* **2012**, *5*, 7927.
[72] V. Chakrapani, F. Rusli, M. A. Filler, P. A. Kohl, *J. Power Sources* **2012**, *205*, 433.
[73] B. Wang, X. Li, B. Luo, X. Zhang, Y. Shang, A. Cao, L. Zhi, *ACS Appl. Mater. Interfaces* **2013**, *5*, 6467.
[74] B. M. Bang, H. Kim, J.-P. Lee, J. Cho, S. Park, *Energy Environ. Sci.* **2011**, *4*, 3395.
[75] Y. Kumai, H. Kadoura, E. Sudo, M. Iwaki, H. Okamoto, Y. Sugiyama, H. Nakano, *J. Mater. Chem.* **2011**, *21*, 11941.
[76] K. Xu, L. Ben, H. Li, X. Huang, *Nano Res.* **2015**, *8*, 2654.
[77] W.-S. Kim, Y. Hwa, J.-H. Shin, M. Yang, H.-J. Sohn, S.-H. Hong, *Nanoscale* **2014**, *6*, 4297.
[78] S. Chen, Z. Chen, X. Xu, C. Cao, M. Xia, Y. Luo, *Small* **2018**, *14*, 1703361.
[79] X. Yu, F. Xue, H. Huang, C. Liu, J. Yu, Y. Sun, X. Dong, G. Cao, Y. Jung, *Nanoscale* **2014**, *6*, 6860.
[80] Z. Lu, J. Zhu, D. Sim, W. Zhou, W. Shi, H. H. Hng, Q. Yan, *Chem. Mater.* **2011**, *23*, 5293.
[81] S. Chen, P. Bao, X. Huang, B. Sun, G. Wang, *Nano Res.* **2013**, *7*, 85.
[82] A. T. Tesfaye, R. Gonzalez, J. L. Coffer, T. Djenizian, *ACS Appl. Mater. Interfaces* **2015**, *7*, 20495.
[83] T. Wada, J. Yamada, H. Kato, *J. Power Sources* **2016**, *306*, 8.
[84] X. Li, M. Gu, S. Hu, R. Kennard, P. Yan, X. Chen, C. Wang, M. J. Sailor, J.-G. Zhang, J. Liu, *Nat. Commun.* **2014**, *5*, 4105.
[85] L. Sun, F. Wang, T. Su, H. Du, *ACS Appl. Mater. Interfaces* **2017**, *9*, 40386.
[86] F. Dai, R. Yi, H. Yang, Y. Zhao, L. Luo, M. Gordin, H. Sohn, S. Chen, C. Wang, S. Zhang, D. Wang, *ACS Appl. Mater. Interfaces* **2019**, *11*, 13257.
[87] R. Miao, J. Yang, Y. Wu, J. Wang, Y. Nuli, W. Lu, *RSC Adv.* **2015**, *5*, 56772.
[88] Q. Li, L. Yin, X. Gao, *RSC Adv.* **2015**, *5*, 35598.
[89] F. Qu, C. Li, Z. Wang, Y. Wen, G. Richter, H. P. Strunk, *Sci. Rep.* **2015**, *5*, 10381.
[90] L. Roiban, S. Koneti, T. Wada, H. Kato, F. J. Cadete Santos Aires, S. Curelea, T. Epicier, E. Maire, *Mater. Charact.* **2017**, *124*, 165.
[91] M.-S. Wang, L.-Z. Fan, M. Huang, J. Li, X. Qu, *J. Power Sources* **2012**, *219*, 29.
[92] R. Zhang, Y. Du, D. Li, D. Shen, J. Yang, Z. Guo, H. K. Liu, A. A. Elzatahry, D. Zhao, *Adv. Mater.* **2014**, *26*, 6749.
[93] G. C. Shivaraju, C. Sudakar, A. S. Prakash, *Electrochim. Acta* **2019**, *294*, 357.
[94] T. Mu, P. Zuo, S. Lou, Q. Pan, H. Zhang, C. Du, Y. Gao, X. Cheng, Y. Ma, H. Huo, G. Yin, *J. Alloys Compd.* **2019**, *777*, 190.
[95] S. Choi, T.-w. Kwon, A. Coskun, J. W. Choi, *Science* **2017**, *357*, 279.
[96] H. Shang, Z. Zuo, L. Yu, F. Wang, F. He, Y. Li, *Adv. Mater.* **2018**, *30*, 1801459.
[97] a) G. Mu, Z. Ding, D. Mu, B. Wu, J. Bi, L. Zhang, H. Yang, H. Wu, F. Wu, *Electrochim. Acta* **2019**, *300*, 341; b) X. Yi, W.-J. Yu, M. A. Tsiamtsouri, F. Zhang, W. He, Q. Dai, S. Hu, H. Tong, J. Zheng, B. Zhang, J. Liao, *Electrochim. Acta* **2019**, *295*, 719; c) M.-S. Wang, G.-L. Wang, S. Wang, J. Zhang, J. Wang, W. Zhong, F. Tang, Z.-L. Yang, J. Zheng, X. Li, *Chem. Eng. J.* **2019**, *356*, 895; d) S.-C. Hou, T.-Y. Chen, Y.-H. Wu, H.-Y. Chen, X.-D. Lin, W.-K. Liew, C.-C. Chang, J.-L. Huang, *ACS Sustainable Chem. Eng.* **2019**, *7*, 2971; e) D. Gueon, J. H. Moon, *Chem. Commun.* **2019**, *55*, 361; f) J.-Y. Li, G. Li, J. Zhang, Y.-X. Yin, F.-S. Yue, Q. Xu, Y.-G. Guo, *ACS Appl. Mater. Interfaces* **2019**, *11*, 4057; g) S.-H. Choi, G. Nam, S. Chae, D. Kim, N. Kim, W. S. Kim, J. Ma, J. Sung, S. M. Han, M. Ko, H.-W. Lee, J. Cho, *Adv. Energy Mater.* **2019**, *9*, 1803121.
[98] a) T. Kennedy, M. Brandon, K. M. Ryan, *Adv. Mater.* **2016**, *28*, 5696; b) H. Wang, H. Song, Z. Lin, X. Jiang, X. Zhang, L. Yu, J. Xu, L. Pan, J. Wang, M. Zheng, Y. Shi, K. Chen, *Nanoscale* **2016**, *8*, 2613; c) L. Wang, D. Liu, S. Yang, X. Tian, G. Zhang, W. Wang, E. Wang, Z. Xu, X. Bai, *ACS Nano* **2014**, *8*, 8249; d) J. H. Cho, S. T. Picraux, *Nano Lett.* **2014**, *14*, 3088; e) S. Jing, H. Jiang, Y. Hu, C. Li, *Nanoscale* **2014**, *6*, 14441; f) X. H. Liu, F. Fan, H. Yang, S. Zhang, J. Y. Huang, T. Zhu, *ACS Nano* **2013**, *7*, 1495.
[99] C. K. Chan, X. F. Zhang, Y. Cui, *Nano Lett.* **2008**, *8*, 307.
[100] C. K. Chan, H. Peng, G. Liu, K. McIlwrath, X. F. Zhang, R. A. Huggins, Y. Cui, *Nat. Nanotechnol.* **2008**, *3*, 31.
[101] C. K. Chan, R. N. Patel, M. J. O'Connell, B. A. Korgel, Y. Cui, *ACS Nano* **2010**, *4*, 1443.
[102] S. Basu, S. Suresh, K. Ghatak, S. F. Bartolucci, T. Gupta, P. Hundekar, R. Kumar, T.-M. Lu, D. Datta, Y. Shi, N. Koratkar, *ACS Appl. Mater. Interfaces* **2018**, *10*, 13442.
[103] a) H. Kim, B. Han, J. Choo, J. Cho, *Angew. Chem., Int. Ed.* **2008**, *47*, 10151; b) F. Dai, R. Yi, H. Yang, Y. Zhao, L. Luo, M. Gordin, H. Sohn, S. Chen, C. Wang, S. Zhang, D. Wang, *ACS Appl. Mater. Interfaces* **2019**, *11*, 13257; c) X. Han, Z. Zhang, G. Zheng, R. You, J. Wang, C. Li, S. Chen, Y. Yang, *ACS Appl. Mater. Interfaces* **2019**, *11*, 714; d) P. Guan, J. Li, T. Lu, T. Guan, Z. Ma, Z. Peng, X. Zhu, L. Zhang, *ACS Appl. Mater. Interfaces* **2018**, *10*, 34283.
[104] A. Magasinski, B. Zdyrko, I. Kovalenko, B. Hertzberg, R. Burtovyy, C. F. Huebner, T. F. Fuller, I. Luzinov, G. Yushin, *ACS Appl. Mater. Interfaces* **2010**, *2*, 3004.
[105] Y. Bie, J. Yang, X. Liu, J. Wang, Y. Nuli, W. Lu, *ACS Appl. Mater. Interfacess* **2016**, *8*, 2899.